

Identifying Trustworthiness Challenges in Deep Learning Models for Continental-Scale Water Quality Prediction

Xiaobo Xia^{1,2} Xiaofeng Liu^{3,4} Jiale Liu⁵ Kuai Fang⁶

Lu Lu² Samet Oymak⁷ William S. Currie^{3,4} Tongliang Liu^{1†}

¹School of Computer Science, University of Sydney, Sydney, NSW 2008, Australia

²Department of Statistics and Data Science, Yale University, New Haven, CT 06511, USA

³Michigan Institute for Data and AI in Society, University of Michigan, Ann Arbor, MI 48105, USA

⁴School for Environment and Sustainability, University of Michigan, Ann Arbor, MI 48109, USA

⁵College of Information Science and Technology, Penn State University, University Park, PA 16802, USA

⁶Department of Earth System Science, Stanford University, Stanford, CA 94305, USA

⁷Department of Electrical Engineering and Computer Science, University of Michigan, Ann Arbor, MI 48109, USA

ABSTRACT

Water quality is foundational to environmental sustainability, ecosystem resilience, and public health. Deep learning models, particularly Long Short-Term Memory (LSTM) networks, offer transformative potential for large-scale water quality prediction and scientific insights generation. However, their widespread adoption in high-stakes decision-making, such as pollution mitigation and equitable resource allocation, is prevented by unresolved trustworthiness challenges including fairness, robustness, uncertainty, interpretability, generalizability, and reproducibility. In this work, we present the first comprehensive, quantitative evaluation of trustworthiness in a continental-scale multi-task LSTM model predicting 20 water quality variables (encompassing physical/chemical processes, geochemical weathering, and nutrient cycling) across 482 U.S. basins. Our investigation uncovers systematic patterns of model performance disparities linked to basin characteristics, the inherent complexity of biogeochemical processes, and variable predictability, emphasizing critical performance fairness concerns. We further propose methodological frameworks for quantitatively evaluating critical aspects of trustworthiness, including robustness, uncertainty, and interpretability, identifying key limitations that could challenge reliable real-world deployment. This work serves as a timely call to action for advancing trustworthy data-driven methods for water resources management and provides a pathway to offering critical insights for researchers, decision-makers, and practitioners seeking to leverage artificial intelligence (AI) responsibly in environmental management.

[†]Corresponding author (tongliang.liu@sydney.edu.au).

Introduction

Water quality is essential for both environmental sustainability and public health, and clean water supports aquatic biodiversity, ecosystem services, and safe drinking water access [1, 2]. However, freshwater contaminants increasingly threaten ecological integrity and human well-being by causing habitat degradation, species loss, and waterborne diseases [3]. In response, substantial efforts have been made, notably with the U.S. investing more than \$1.9 trillion since 1960 to reduce pollution in rivers, lakes, and other surface waters, a commitment exceeding most other U.S. environmental initiatives [4]. Assessment of water quality is typically based on sample collection that is expensive and labor-intensive, while also producing highly heterogeneous datasets with limited scalability [5, 6].

Artificial Intelligence (AI) has provided a new set of tools with the potential to make progress on these challenges. In particular, deep neural networks such as long short-term memory (LSTM) models, renowned for their ability to capture long temporal dependencies in time series data, have become the most widely applied machine learning models in hydrological modeling [7, 8, 9]. However, their application to predict a wide range of water quality variables over space and time, especially across large scales, remains nascent and contentious. In addition, practitioners often distrust “black-box” machine learning frameworks, despite improved predictive accuracy relative to simple statistical models, due to concerns about explainability and interpretability [10]. This skepticism arises partly because of the high stakes involved: water quality management decisions carry profound societal implications, from infrastructure design to pollution mitigation. To be adopted and used, AI-based models need to be not only accurate but also trustworthy.

Trustworthiness in AI broadly encompasses multiple critical aspects, including but not limited to their fairness in both modeling processes and outcomes, robustness against noise and adversarial disruption, uncertainty quantification, explainability of model decisions, generalizability to unseen conditions, and reproducibility of research [11, 12, 13, 14, 15]. While building trustworthy data-driven methods has long been a vision and key development goal in many fields of science and engineering [16], such as healthcare, autonomous driving, sentiment analysis, and climate science [17, 18, 19, 20], their adoption in water quality research lags considerably behind. Current deep learning research in water quality has largely focused on improving performance metrics (e.g., predictive accuracy), often overlooking these essential trustworthiness considerations. For deep learning models to become more widely adopted in guiding watershed management and decision-making, especially when combined with climate and socioeconomic uncertainties, multiple aspects of trustworthiness need to be more carefully evaluated and justified [21].

In this study, we present the first comprehensive, quantitative evaluation of trustworthiness in LSTM-based prediction of water quality variables. This investigation extends beyond conventional predictive accuracy

metrics to address persistent concerns: (1) How does model performance vary across water quality variables and basin types? (2) How robust is the model when exposed to outliers, random noise, and adversarial perturbations? (3) How does uncertainty in model predictions vary across variables, and are certain variables disproportionately impacted? (4) Do feature importance analysis methods yield consistent results in identifying key drivers? (5) Can the model generalize effectively to unmonitored basins? To answer these questions, we first train a multi-task LSTM model using 37 years of water quality observations, hydroclimate forcings, and static basin attributes across 482 U.S. basins (see Methods) to predict 20 water quality variables representing physical/chemical, geochemical weathering, and nutrient cycling processes. We then evaluate the model's robustness under various data corruption scenarios, quantify prediction uncertainty using the Monte Carlo dropout approach [22], and compare feature importance derived from ablation studies and the Traverse method. Our main contribution is defining and demonstrating a reproducible trust benchmarking protocol, which is urgently needed yet missing in this domain. The proposed evaluation framework is model-agnostic and can be readily extended to other architectures or application domains.

Results and Discussion

Challenges in predicting management-critical water quality variables

Our continental-scale multi-task LSTM model (Fig. 1a) exhibits a wide range of performance accuracy (as measured by Kling-Gupta Efficiency, KGE, see Methods) across different water quality variables. Overall, the model achieves high median KGE values for Temp (temperature, 0.94) and DO (dissolved oxygen, 0.80) (Fig. 1c). It also demonstrates moderate predictive accuracy for variables associated with geochemical weathering processes, including Cond (conductivity), Mg^{2+} , K^+ , and SiO_2 (median KGE: 0.62-0.76). However, it fails to capture the dynamic variability of CO_2 , pH, and TSS (total suspended sediments) and underperforms in nutrient-related variables, particularly NH_x and PO_4^{3-} (median KGE < 0.4). To further assess model performance, we evaluated TP predictions at an agriculturally intensive basin that includes additional daily observations not present in either the training or testing datasets. At this site, the model achieves a relatively high KGE of 0.63 for the testing periods, exceeding the nationwide median (0.46). However, the model's daily predictions demonstrate significant discrepancies when compared with these additional daily measurements (Fig. 1d). This suggests that while the model trained with a nationwide dataset may achieve reasonable overall accuracy at given testing samples, it might not be able to reliably reproduce finer-scale nutrient dynamics at certain basins.

In fact, nutrients (such as various forms of nitrogen and phosphorus) were among the most challenging variables for both the LSTM and the benchmark model, showing relatively lower predictive performance over-

all [23]. These difficulties arise likely because nutrient concentrations often spike or fluctuate in response to episodic events (e.g., fertilizer applications, storm runoff) and involve reactive processes in both soils and streams. Phosphorus concentrations are also sensitive to long-term legacies of P accumulation in soils. The LSTM, which primarily learns from historical input-output patterns, struggles to represent the underlying biogeochemistry processes or differences related to longer-term human impacts. Additionally, routine water quality monitoring for nutrient variables is typically infrequent (e.g., weekly or monthly grab samples), causing responses to episodic events and associated fast dynamics to be under-sampled and thus underrepresented in training data. These limitations in water sampling also undermine trust in modeling nutrients where accurate predictions are often most needed for environmental management.

Fairness concerns due to land use heterogeneity, data availability, and variable simplicity

In water quality prediction, fairness refers to achieving consistent predictive performance across diverse geographic, environmental, and socio-economic contexts, ensuring no basin types are systematically disadvantaged due to inherent biases or disparities in data.

Our findings reveal notable disparities across different land use conditions (Fig. S2), raising potential fairness concerns. Specifically, temperature predictions show reduced accuracy (lowest median KGE) in undeveloped western mountain basins, suggesting an inherent bias likely due to complex snowmelt-driven thermal variability that disproportionately impacts these regions. Among weathering-related variables, SiO_2 , K^+ , and Cl^- exhibit highest KGE values in urban basins, whereas other weathering parameters (e.g., Cond, Ca^{2+} , Mg^{2+} , Na^+ , and SO_4^{2-}) demonstrate higher skill in undeveloped and agricultural basins but lower in urban and mixed basins. Predictions of nutrient variables, such as TN, NO_3^- , and TP, are more reliable in agricultural and urban basins, probably due to frequent fertilizer applications and human activities (e.g., discharge of wastewater treatment plants) yield more consistent and predictable concentration-runoff (C-Q) relationships. In contrast, undeveloped basins show the poorest nutrient predictions. NPOC is an exception, which achieves the best performance in undeveloped basins, a pattern consistent with terrestrial carbon export mechanisms rather than anthropogenic point sources.

We further examined how the training data amount influenced model performance but found no consistent relationship across variables (Fig. 1e). For instance, several weathering variables achieve moderate accuracy (median KGE > 0.6) even with fewer training samples, whereas nutrient-related variables exhibit low performance even when trained with more data than the former. However, a “simplicity index” adapted from [23], which quantifies the proportion of variance in water quality dynamics explained by linear relationships with

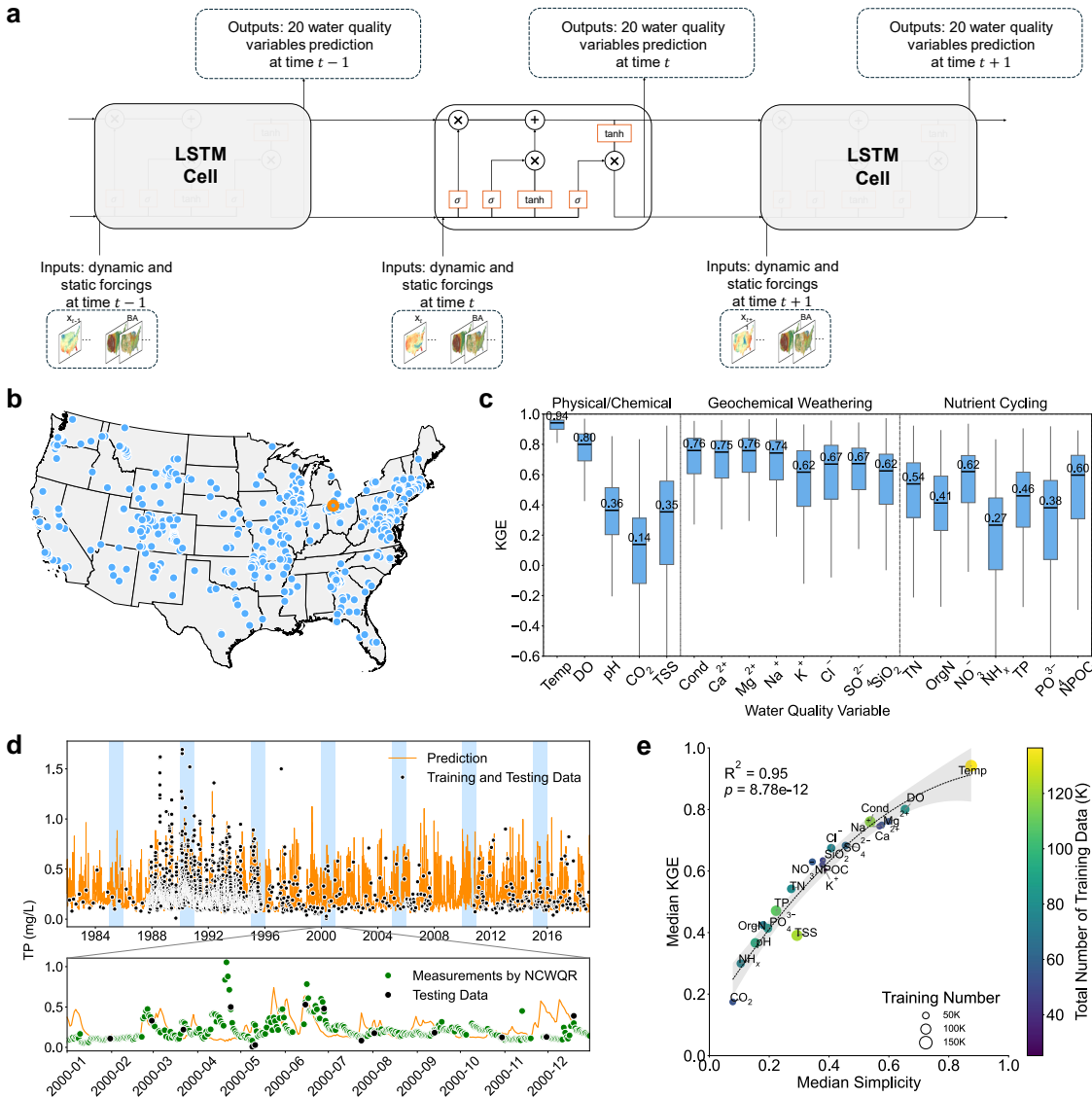


Fig. 1. Multi-task LSTM model architecture and performance for water quality predictions across the continental United States (CONUS). a. Schematic representation of the multi-task LSTM model to predict 20 water quality variables simultaneously by leveraging time-series hydroclimate forcings and static basin attributes as inputs. **b.** Spatial distribution of 482 riverine water quality monitoring sites (blue dots) across CONUS included in this study. **c.** Boxplot of Kling-Gupta Efficiency (KGE) values for the testing periods (1985, 1990, 1995, 2000, 2005, 2010, and 2015) across 20 predicted water quality variables associated with physical/chemical properties, geochemical weathering processes, and nutrient cycling, respectively. The boxplots display the median (central line), interquartile range (IQR, represented by the boxes spanning the first (Q1) to the third quartile (Q3)), and whiskers extending to $Q1 - 1.5 \times IQR$ and $Q3 + 1.5 \times IQR$. The number marked on the box refers to the median. **d.** Example time series showing model predictions, testing samples, and additional daily observations (excluded from training and testing samples) of TP (total phosphorus) collected by the National Center for Water Quality Research (NCWQR) at the Maumee River in

Waterville, OH (indicated by the orange circle star in panel b) during the testing year 2000. **e.** Relationships between model performance, simplicity, and the total number of training samples across 20 water quality variables. Model performance is represented by the median KGE across CONUS, while the simplicity index measures the proportion of variance in water quality explained by linear relationships with runoff and annual cycles [23]. The size and color of each dot indicate the number of training samples, with larger, yellow dots representing more data and smaller, blue dots indicating less data. The grey shade represents the 95% confidence interval of the polynomial regression line.

runoff and annual cycles (see Methods), shows a strong correlation with model performance across variables ($R^2 = 0.95$, $p < 0.001$; Fig. 1e), suggesting that model performance fairness largely depends on the inherent predictability of water quality variables, driven by hydrological or seasonal patterns. Variables characterized by higher simplicity, for example, weathering-related parameters, achieve reliable predictions despite sparse training data. In contrast, nutrient variables exhibiting low simplicity may require more frequent sampling to achieve equitable predictive performance, as demonstrated in agricultural basins, which have both greater data coverage (the ratio of days measured to the total number of days between 01/01/1982 and 12/31/2018; Fig. S3) and better performance (Fig. S2). These findings align with research indicating that LSTMs benefit from dense temporal sampling to resolve human-influenced signals [24]. However, in undeveloped basins, nutrient predictions remain problematic due to compounding challenges: limited data coverage (Fig. S3), inherently low simplicity (Fig. S4), and possible signal masking by higher concentrations from the urban, mixed, and agricultural basins. This inequity disproportionately impacts undeveloped basins, resulting in prediction biases and fairness concerns that must be addressed through targeted sampling strategies and methodological improvements.

Although our CONUS LSTM model was trained with diverse catchment attributes as static inputs to account for differences among basins, many auxiliary influences were either not quantified or not available at the necessary resolution. For instance, temporally and spatially resolved inputs like fertilizer application rates/-timing, livestock impacts, or industrial discharges were absent from the training data. As a result, the model could not learn the true impact of those factors on water quality, leading to site-specific errors. Catchments with intensive agriculture or urbanization may exhibit nutrient concentration patterns closely tied to land management practices or human activities, whereas forested basins might show more dampened, baseflow-driven patterns. Such divergent behaviors are difficult for the LSTM to reconcile under a unified modeling approach, especially if the important drivers with sufficient resolution are not explicitly included as inputs.

Addressing these fairness gaps is important especially for high-stakes applications involving regulatory compliance and ecosystem protection. Enhanced sampling/monitoring networks, incorporation of key auxiliary inputs, and advanced modeling approaches are needed to ensure fairness and trust in AI-driven water qual-

ity predictions, supporting equitable water quality management and effective decision-making across diverse environmental and socio-economic settings.

Limited robustness to outliers, random noise, and adversarial disruptions

Robustness against outliers. Our results (Fig. 2a) reveal that LSTM models exhibit pronounced sensitivity to outliers, a critical limitation given the prevalence of extreme values in environmental datasets (e.g., storm-driven pollutant spikes, sensor malfunctions, and measurement errors). When 10% of synthetic outliers were introduced into input features, more than 50% of basins exhibited a performance decrease (the median percentage reduction in KGE relative to the baseline) of over 21.7% in NH_x predictions and 19.2% in CO_2 predictions. Variables such as Ca^{2+} , NPOC, DO, and temperature showed minimal degradation (< 2%). A strong positive correlation ($r = 0.87, p < 0.001$) between the median KGE from the baseline model and the median percentage reduction in KGE indicates that the variables with higher initial predictive accuracy exhibit less sensitivity to input outliers (Fig. 2b). However, outliers injected directly into water quality measurements cause disproportionately greater impacts. Specifically, for 18 out of 20 variables, more than half of the basins show KGE reductions exceeding 50% except for temperature and DO (Fig. 2a). Surprisingly, variables associated with geochemical weathering demonstrate a greater overall performance decline than nutrient-related variables. This pronounced impact on weathering-related variables also disrupts the previously observed correlation between the baseline median KGE and the percentage change in KGE ($r = 0.11$, Fig. 2b). These findings imply that this crisis of trust cannot be resolved through improving the predictive accuracy alone. Instead, it requires a paradigm shift toward data-centric environmental AI, where rigorous quality control (e.g., outlier detection, sensor calibration) during data preprocessing is prioritized before training the model.

Robustness against random noise. Similar to the effects observed in the outlier injection experiments, our results also show that LSTM models are sensitive to random noise, with varying degrees of impact across different water quality variables (Fig. 2c). Likewise, the performance degradation is significantly higher when noise is applied to target water quality variables compared to input features ($p < 0.001$), except for TSS, OrgN, NH_x , and TP. Strong correlations between the baseline median KGE and the percentage change of KGE ($r = 0.91$ for input features and $r = 0.76$ for water quality variables, Fig. 2d) suggest that enhancing baseline predictive accuracy could improve robustness to random noise in input features and target variables.

Robustness against adversarial disruptions. Unlike random noise, adversarial perturbations are systematically optimized to maximize prediction errors, making them a critical stress test for model robustness. We generated adversarial noise to input features using Projected Gradient Descent (PGD) (as detailed in the

Methods). Our results indicate that when 10% and 20% adversarial noise were introduced to corrupt input features, more than 50% of basins exhibited a KGE reduction over 27.1% in TSS predictions, 22.1% in CO₂ predictions, and 16.5% in NH_x predictions (Fig. 2e). The least affected variables are temperature and DO with 2.3% KGE decline, further demonstrating their relatively higher robustness to various perturbations. Geochemical weathering variables exhibit greater robustness to adversarial noise compared to nutrient variables. Specifically, the median KGE decline for these variables range from 5.1% for Mg²⁺ to 9.7% for K⁺, which is consistently lower than the degradation observed in nutrient cycling variables (excluding NPOC), where declines range from 9.6% for PO₄³⁻ to 16.5% for NH_x. Similarly, a strong positive correlation ($r = 0.84$, $p < 0.001$; Fig. 2f) between the median baseline KGE and the percentage reduction of KGE further reveals that variables with initially lower performance would be more sensitive to input adversarial noise. This finding also highlights the importance of considering variable-specific vulnerabilities when evaluating model robustness, as certain variables (e.g., nutrient variables) are inherently more susceptible to adversarial noise, potentially increasing safety risks in decision-making (e.g., Total Maximum Daily Load assessment).

In summary, our results reveal that LSTMs face significant robustness challenges when exposed to data perturbations common in environmental monitoring and management. While improving baseline predictive performance can enhance model robustness to some extent, it does not fully mitigate the impact of extreme data disruptions (e.g., outliers in measured water quality variables). Addressing this issue requires an integrated data-centric and model-centric approach. On the data side, implementing stringent quality assurance and control (QA/QC) protocols for sensor/sample data is necessary to reduce noise and errors in training datasets. Leveraging domain knowledge to identify variables most susceptible to corruption can further improve model performance by allowing targeted preprocessing efforts. On the model side, for instance, integrate adversarial training [25] or distributionally robust optimization [26] to improve resilience against targeted attacks. These methodological improvements are crucial for ensuring that AI-driven water quality models can be reliably deployed in operational settings, where the model predictions could be used to inform environmental risk assessment, regulatory enforcement, and decision-making.

While this study focuses on LSTM architectures to benchmark robustness challenges in water quality research, it also highlights the need for the broader community to investigate whether these vulnerabilities are unique to LSTMs or inherent to deep learning approaches more broadly. Future research should also compare LSTMs with alternative deep learning architectures, such as Transformer-based models [27], to disentangle limitations associated with sequential modeling from fundamental deep learning vulnerabilities (e.g., sensitivity to input perturbations, overreliance on training distributions). For instance, Transformer models, which replace recurrent connections with self-attention mechanisms, may exhibit distinct robustness due to their ability to capture any long-term pair-wise dependencies and parallelize training. Such comparisons may be

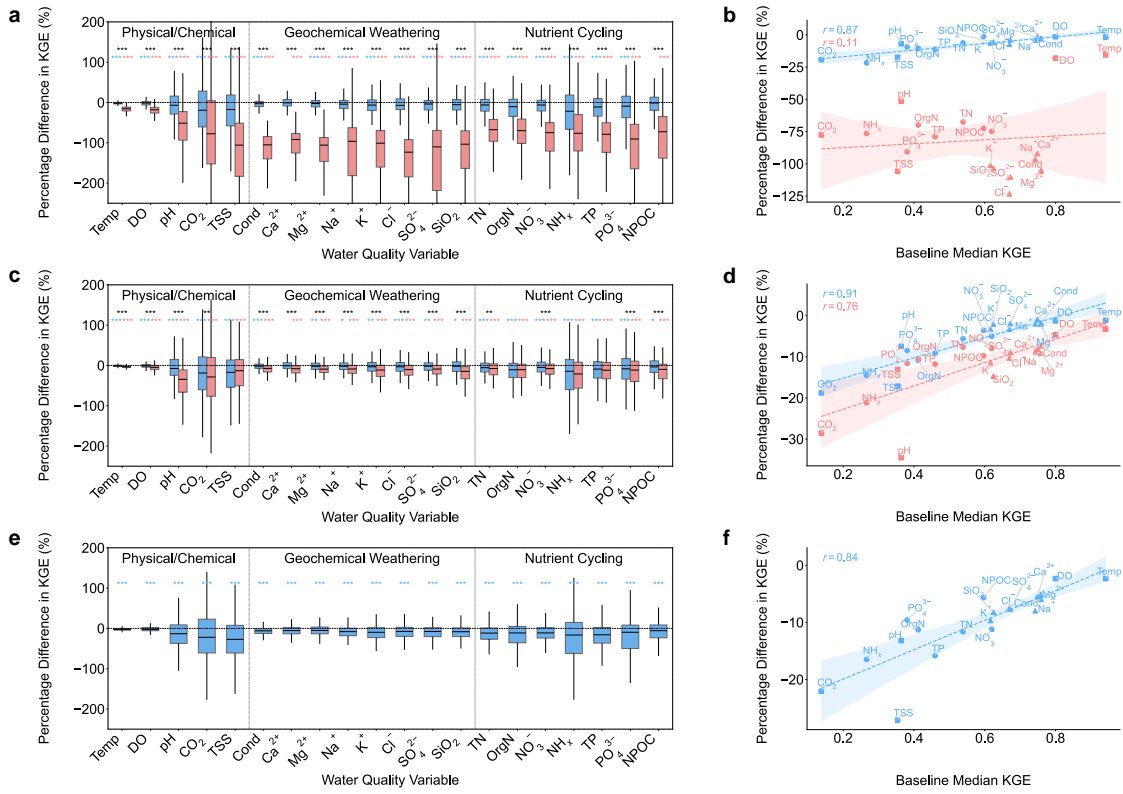


Fig. 2. Impact of observational data corruption on LSTM model performance. Blue denotes corruption applied to input features, whereas red denotes corruption applied to water quality variables. **a** and **b** show the median percentage change in KGE relative to the baseline when outliers are introduced and its correlation with initial (baseline) KGE, respectively. **c** and **d** present the effects of random noise, and **e** and **f** show the effects of adversarial disruptions. In **a**, **c**, and **e**, the boxplots show the median (central line), interquartile range (IQR, represented by the boxes spanning the first (Q1) to the third quartile (Q3)), and whiskers extending to $Q1 - 1.5 \times IQR$ and $Q3 + 1.5 \times IQR$; Wilcoxon Signed-Rank tests assess whether the median percentage change in KGE is significantly less than zero (indicated by blue or red stars) and whether corruption of water quality variables leads to a significantly greater KGE reduction than corruption of input features (indicated by black stars). Significance levels are: *** $p < 0.001$, ** $p < 0.01$, and * $p < 0.05$. In **b**, **d**, and **f**, triangles represent geochemical weathering variables, circles denote nutrient variables, and squares denote physical-/chemical variables. Pearson correlation quantifies the relationship between baseline median KGE and the percentage change in KGE, reflecting how initial performance relates to vulnerability under data corruption. The shaded region around the regression line refers to the 95% confidence interval.

able to provide insights into whether architectural innovations can help mitigate vulnerabilities to outliers, random noise, and adversarial attacks.

Higher prediction uncertainty in management-critical water quality variables

Accurate and reliable uncertainty quantification is essential for deploying deep learning models for water quality management. Our Monte Carlo dropout analysis reveals a concerning trend: variables critical for ecosystem health, such as NH_x , PO_4^{3-} , and TSS exhibit the highest uncertainty (median SD of KGE > 0.08 ; Fig. 3a), followed by variables associated with the weathering process (median SD of KGE: 0.06-0.08), while physical/chemical variables like temperature and DO show the least uncertainty (median SD of KGE < 0.02). The strong negative relationship between predictive performance (median KGE) and uncertainty ($r = -0.62$, $p < 0.001$; Fig. 3b) demonstrates that the most management-critical variables are also the least reliably predicted.

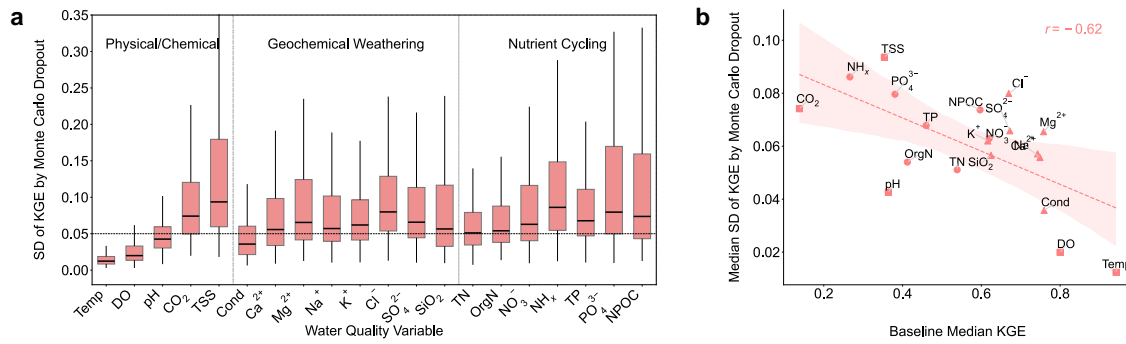


Fig. 3. Relationship between model predictive performance and uncertainty. **a.** The uncertainty of model predictions across different water quality variables, quantified as the standard deviation (SD) of the Kling-Gupta Efficiency (KGE) obtained from Monte Carlo dropout across 50 simulations (see Methods). The boxplots show the median (central line), interquartile range (IQR, represented by the boxes spanning the first (Q1) to the third quartile (Q3)), and whiskers extending to $Q1 - 1.5 \times \text{IQR}$ and $Q3 + 1.5 \times \text{IQR}$. **b.** A strong negative correlation ($r = -0.62$, $p < 0.001$) between the baseline median KGE across 482 basins and the median uncertainty (SD of KGE), indicating that water quality variables with lower predictive performance tend to exhibit higher uncertainty. The shaded region around the regression line represents the 95% confidence interval.

The increased uncertainty for nutrient and weathering variables is likely due to their dependence on nonlinear, temporally variable processes that are poorly constrained by current model architectures and input data. Unlike temperature and DO, which exhibit strong seasonality and response predictably to meteorological drivers such as air temperature, variables like NH_x and PO_4^{3-} are impacted by complex nonlinear biogeochemical processes, including sediment adsorption-desorption and microbial mineralization. In addition, monitoring data for nutrients and weathering variables are sparser compared to temperature and DO, particularly in undeveloped basins (Fig. S3), which also limits the model's ability to learn complex patterns and

therefore amplifies uncertainty. Adopting uncertainty-aware loss functions [28, 29, 30] and early uncertainty estimation strategies [31] can help prioritize reliable predictions for high-stakes variables.

Inconsistent feature importances challenge model interpretability

Feature importance analysis remains a critical focus in model explainability research. In the context of water quality prediction, interpreting model decisions and identifying key drivers are critical for both scientific understanding and management applications. However, our analysis reveals notable inconsistencies in feature importance estimates derived from two widely used approaches. Specifically, we compared the Traverse method [32], which evaluates all possible input combinations, and Ablation studies [33, 34], which remove one feature group from the full model (see Methods). Using both approaches, we assessed how meteorological forcing (M), runoff (Q), rainfall chemistry (RC), vegetation indices (V), and basin attributes (BA) contribute to LSTM performance across multiple water quality variables.

Both methods consistently identify runoff as the most critical driver for weathering, nutrient, and the majority of physical/chemical variables (excluding temperature and DO). More than half of basins exhibit significant KGE reduction when runoff is excluded (median KGE reductions: 0.01-0.27 by the Traverse method and 0.01-0.12 by the Ablation; $p < 0.001$; Fig. 4), reflecting the dominant mechanistic role of runoff in particulates and solutes transport. Meanwhile, basin attributes (BA), though static, also show significant importance (median KGE reductions ranging from 0.01 to 0.09 by the Traverse method and 0.01 to 0.08 by the Ablation; $p < 0.001$), likely encoding baseline water quality conditions defined by various basin characteristics, which provides critical context for short-term dynamics driven by runoff and meteorological forcing [32].

In contrast, meteorological forcing (M) exhibits inconsistent feature importance estimates between the two methods. Both approaches highlight M as the primary driver for temperature and DO dynamics, aligning with previous findings [32] that highlight the strong influence of air temperature on oxygen dynamics governed by solubility, photosynthesis, and other biological activities. However, the Ablation approach underestimates M's importance for other variables, showing no significant KGE reduction ($p > 0.05$; Fig. 4). Further analysis indicates that specifically when the runoff is included, meteorological information appears redundant (Fig. S5), which was also demonstrated in a previous study [23]. A similar pattern emerges for rainfall chemistry (RC) and vegetation indices (V): the Ablation suggests nonsignificant importance for most variables (except for nitrate), whereas the Traverse method reveals significant median KGE declines for many weathering parameters ($p < 0.001$; Fig. 4).

These inconsistencies align with previous findings that in scenarios with substantial feature overlap, a model may favor one subset of variables without fully reflecting real-world dependencies, causing Ablation to un-

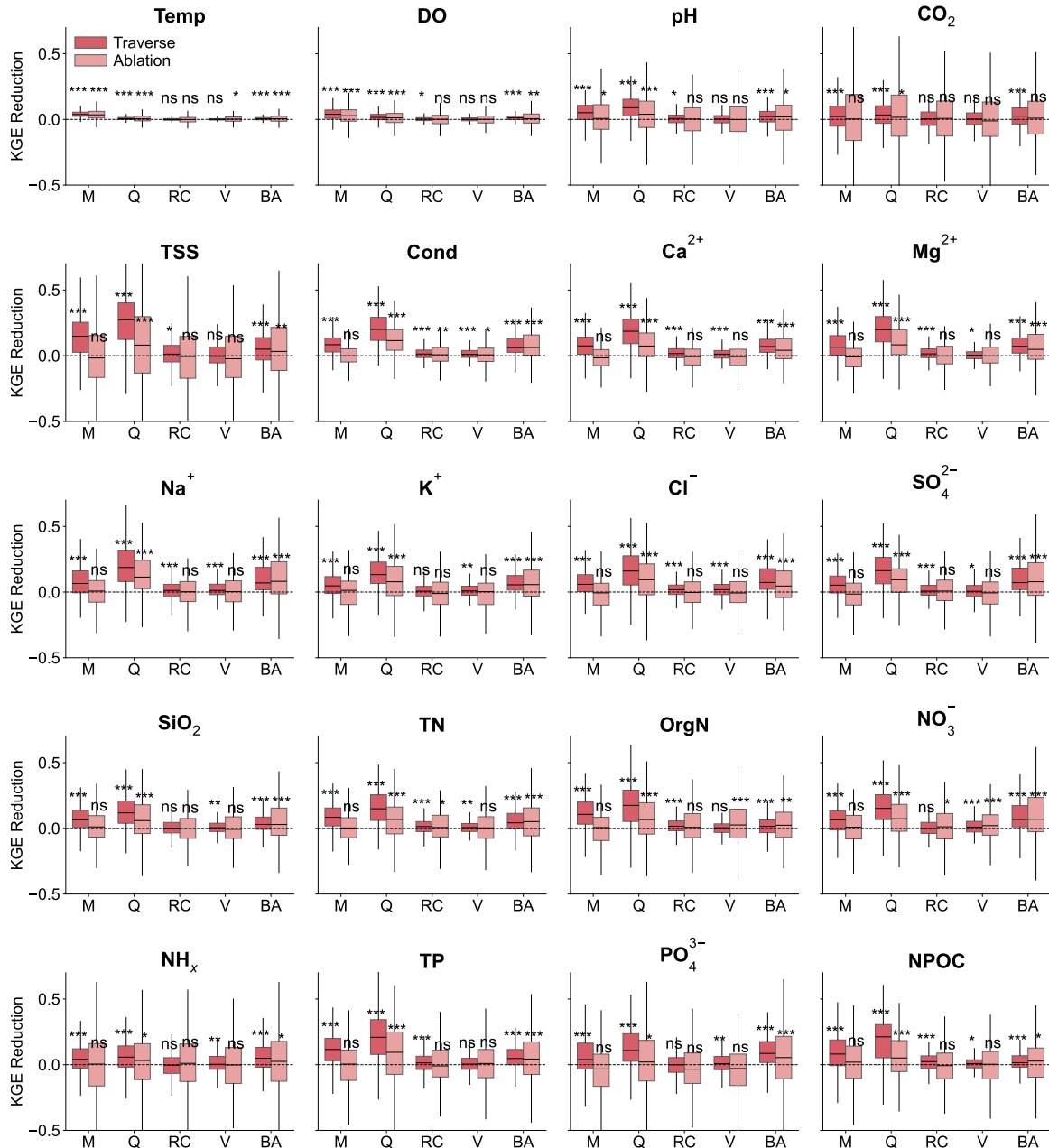


Fig. 4. Feature importance comparison across five groups: meteorological forcings (M), runoff (Q), rainfall chemistry (RC), vegetation indices (V), and basin attributes (BA). Feature group details are provided in Methods. In the Ablation approach (light red boxes), feature importance is quantified by the reduction in Kling-Gupta Efficiency (KGE) when that group is removed from the full model. In the Traverse approach (dark red boxes), the feature importance of each group is calculated as the average KGE reduction across all possible feature group combinations with and without the target group (see Methods). The boxplots show the median (central line), interquartile range (IQR, represented by the boxes spanning the first (Q1) to the third quartile (Q3)), and whiskers extending to $Q1 - 1.5 \times IQR$ and $Q3 + 1.5 \times IQR$. For both methods, Wilcoxon signed-rank tests were performed to assess whether median KGE reductions across 482 basins significantly exceeded zero (black stars; *** $p < 0.001$, ** $p < 0.01$, * $p < 0.05$, and "ns" for $p \geq 0.05$).

derestimate the value of certain input features [35, 36]. The Traverse method evaluates a feature group's contribution across all subsets (e.g., M alone, M + Q, M + BA, etc), isolating standalone and interactive effects. In contrast, Ablation measures only the marginal loss from removing a group from the full model, where overlapping signals (e.g., precipitation information embedded in runoff through the runoff generating process) mask true importance. However, underestimating indirect contributions of meteorological forcing (via Ablation) risks overlooking climate-sensitive drivers of eutrophication, particularly in basins where precipitation extremes amplify runoff-sediment interactions.

It is also noted that while the Traverse approach provides a more comprehensive attribution evaluation, its computational cost scales exponentially with features (e.g., 32 combinations for 5 feature categories in this study; 2^{49} infeasible for individual basin attributes). In addition, although the brute-force nature of the Traverse method captures interactions, it lacks the formal weighting or ordering perspective present in certain game-theoretic approaches, such as Marginal Contribution Feature Importance [36] and Shapley values [37].

Our study intentionally focused on two widely used and computationally feasible methods, Traverse and Ablation, that are effective for evaluating model trustworthiness. The goal is not to provide an exhaustive comparison of all interpretability techniques. While other methods such as SHAP [37] and Integrated Gradients [38] are valuable methods and are also used for feature importance analysis, their omission does not diminish the validity or relevance of the trust benchmarking framework we propose.

Generalizability

Our spatial training-testing split results (Fig. S6) indicate that the LSTM model exhibits poor generalizability to “ungauged” basins for most water quality variables, except for temperature and dissolved oxygen, which achieve relatively high KGE values of 0.88 and 0.71, respectively. These findings highlight the challenge of learning spatially transferable patterns, particularly for those geochemical and nutrient-related variables.

The sparsity of water quality observations, with many basins having limited or no historical data, further compounds this challenge. In practice, a trustworthy model must generalize reasonably well to data-scarce basins, enabling reliable predictions where in situ monitoring is unavailable. However, a fundamental limitation of deep learning models lies in their limited capacity to generalize beyond training conditions. Unlike process-based models that embed mechanistic relationships (e.g., reaction kinetics and advection-diffusion), LSTMs rely on statistical patterns in training data, which are often sparsely measured for critical water quality variables or inadequately capture extreme hydrological events such as floods and droughts [39]. As climate change continuously increases the frequency and severity of such extremes [40], the inability of purely data-

driven models to extrapolate beyond their training distribution poses a critical challenge for trustworthy water quality prediction.

Knowledge-Informed Deep Learning (KIDL) has emerged as a promising strategy to address these challenges. By incorporating domain knowledge, such as mass conservation and transport dynamics into the model’s architecture and learning process, KIDL enforces physically plausible behavior even under unseen conditions. For example, Agrawal et al. [41] integrated a physical “flow-gate” mechanism into an LSTM model to explicitly model hysteresis between discharge and solute dynamics, which improved predictions of nine stream solutes (RMSE reduced by 1-32% compared with standard LSTM). Hybrid modeling approaches have also shown success by combining physics-based simulations with physics-informed loss functions to ensure predictions align with foundational physical principles, as demonstrated in lake temperature modeling [42]. While these studies illustrate the potential of KIDL, its application in water quality research remains limited, compared to its use in hydrology and other scientific fields [43, 44, 45]. In addition, large-scale pre-trained foundation models offer complementary pathways to enhance generalizability. These models have the ability to transfer learned knowledge to unseen tasks via few-shot (minimal samples) or zero-shot (no samples) learning [46]. For example, a model pretrained on extensive, diverse datasets, even those unrelated specifically to water quality, may effectively generalize to predict water quality variables in ungauged basins using limited local measurements. By decreasing dependence on sparse, domain-specific data, pretrained models have the potential to substantially improve resilience to distribution shifts driven by climate change.

Reproducibility

Reproducibility in AI research is essential for verifying findings [11], and it has increasingly become a requirement for publication within AI communities [47]. While AI models show significant promise for water quality research, progress in this domain is hindered by limited openness and transparency. A relatively small number of studies in this field provide full public access to their original data, models, and code, creating barriers to reproducibility, benchmarking, and collaboration. The commitment to reproducibility is more than just a verification of research [11]; it is a critical step to building trust in adopting AI tools in this domain.

Methods

Water quality data and basin selection

In this work, we study 20 water quality variables regularly measured by the U.S. Geological Survey (USGS). These variables are extracted from the USGS National Water Information System (NWIS) database [48] and represent various aspects of stream water quality dynamics, including physical and chemical processes, geo-

chemical weathering, and nutrient cycling. Variables related to stream physical/chemical processes include temperature (Temp, °C), dissolved oxygen (DO, mg/L), pH, total dissolved CO₂ (mg/L), and total suspended sediment concentration (TSS, mg/L). Variables associated with geochemical weathering include conductivity (Cond, uS/cm at 25°C), dissolved silica (SiO₂, mg/L), calcium (Ca²⁺, mg/L), sodium (Na⁺, mg/L), potassium (K⁺, mg/L), magnesium (Mg²⁺, mg/L), sulfate (SO₄²⁻, mg/L), and chloride (Cl⁻, mg/L). Variables related to nutrient cycling include total nitrogen (TN, mg/L), organic nitrogen (OrgN, mg/L as N), nitrate (NO₃⁻, mg/L as N), ammonia and ammonium (NH_x, mg/L as NH₄⁺), total phosphorus (TP, mg/L as P), orthophosphate (PO₄³⁻, mg/L as PO₄³⁻), and non-particulate organic carbon (NPOC, mg/L). Water quality data are from samples collected on a daily basis over a 37-year period, from January 1, 1982, to December 31, 2018, across 482 basins in the continental United States (CONUS) (Fig. 1b). These basins were selected based on relatively complete water quality records using a sequential screening process as follows: (1) Basins are included in the Geospatial Attributes of Gages for Evaluating Streamflow version II (GAGES-II) [49], a comprehensive dataset maintained by the USGS that provides geospatial data and classifications for over 9,000 stream gages, including basin boundaries. (2) Basins with records in which at least one water quality variable was measured for more than 200 days were retained, while basins with records not meeting this criterion were discarded. (3) We further excluded basins that measured only water temperature and specific conductance. Following this selection process, 482 basins remained for model training and evaluation. Table S1 summarizes the statistics of the selected water quality variables and the average number of observations per site over the study period.

Model input

In addition to water quality variables, inputs to our LSTM model analysis comprised both time-series forcings and static basin attributes. The time-series forcings are categorized into four groups: runoff, meteorological variables, vegetation indices, and rainfall chemistry. Runoff was derived as streamflow measured by the USGS divided by the basin area. Meteorological variables, including precipitation, maximum and minimum temperature, solar radiation, specific humidity, and reference evapotranspiration (grass and alfalfa, calculated using the ASCE Penman-Montieth method), were from the gridMET dataset [50]. These data were spatially aggregated for each basin using basin boundaries from the GAGES-II database. Vegetation indices, including leaf area index (LAI), net primary production (NPP), and fraction of absorbed photosynthetically active radiation (FAPAR), were obtained from the Global Land Surface Satellite (GLASS) dataset [51]. The GLASS dataset provides 8-day estimates with a spatial resolution of 0.05°. To align with the daily modeling time step, these data were interpolated to daily values using cubic splines and spatially aggregated by basin boundaries. Rainfall chemistry data were extracted from the National Atmospheric Deposition Program/National Trends Network (NADP/NTN) [52], which reports weekly measurements of sulfate, nitrate, chloride, ammonium,

potassium, sodium, calcium, and magnesium, pH, and specific conductivity. To construct a daily time series, weekly concentrations at each NTN station were assumed to be constant over each week. Rainfall chemistry for each basin was assigned using the nearest NTN station, with the distance between the basin center and the corresponding NTN station included as an additional input feature. To capture temporal and cyclical patterns in the data, we also incorporated three time-related variables: datenum (T), the sine of the time variable ($\sin T$), and the cosine of the time variable ($\cos T$). The datenum (T) represents the number of days relative to January 1, 2000, with negative values for dates before this reference point and positive values for dates after.

Based on domain knowledge and insights from previous modeling studies [32, 53, 23], we identified 49 static basin attributes from the GAGES-II database as additional features. These static basin attributes encompass a wide range of phenomena and basin characteristics including topographic characteristics, the average percentage of total precipitation occurring as snow in the basin, stream hydrologic characteristics, dam information, land cover percentages, soil properties, geological features, nutrient application rates (nitrogen and phosphorus) from agriculture in the basin, and ecological classifications, as detailed in Table S2.

The selected 482 basins span multiple geographic regions and exhibit a wide range of hydrologic characteristics, hydroclimatic conditions, and land use patterns, reflecting the broad geographical diversity and regional representativeness of the water systems included in the study. These basins include 126 headwater basins (26%) with 1st to 3rd stream orders, 280 medium-sized basins (58%) with 4th to 6th stream orders, and 76 larger basins (16%) with the 7th stream order or higher. The mean (median) drainage areas are 89.03 (108.54) km^2 for headwater basins, 3,224.07 (5,474.93) km^2 for medium basins, and 20,520.4 (13,062.6) km^2 for larger basins. Hydroclimatic conditions vary significantly across the basins. Mean annual precipitation ranges from 213.5 to 2,748.4 mm/year, with an overall mean (median) of 976.8 (985.9) mm/year. Mean annual temperatures range from -1.3 to 22.9°C, with a mean (median) of 10.5 (10.1) °C. Mean annual runoff values range from 1.6 to 2,181.5 mm/year, with a mean (median) of 348.6 (318.2) mm/year. In addition to hydrologic and climatic variability, the basins exhibit diverse land use patterns. According to classification criteria established by the USGS [54], agricultural basins (AG) were defined as those with more than 50% agricultural land (PLANTNLCD06 in the GAGES-II database) and less than or equal to 5% urban land (DE-VNLCD06 in the GAGES-II database). Undeveloped basins (UD) were identified as having less than or equal to 5% urban land and less than or equal to 25% agricultural land. Urban basins (UR) were classified as those with more than 25% urban land and less than or equal to 25% agricultural land, while mixed basins (MX) included all other combinations of urban, agricultural, and undeveloped land. Among the selected basins, 3.1% were classified as AG, 11.2% as UR, 35.1% as UD, and 50.6% as MX, respectively (Fig. S1).

Multi-task LSTM model training and evaluation

The Long Short-Term Memory (LSTM) model is a prominent member of Recurrent Neural Network (RNN) models designed to leverage sequential information for time series prediction [55]. Unlike standard RNNs, which suffer from the vanishing gradient problem when capturing long-term dependencies [56]. LSTM incorporates a memory mechanism to address this limitation. This mechanism, involving “memory states” and “gates”, allows the model to regulate what information to retain or discard over time, enabling more effective learning of temporal patterns. In this work, we trained a multi-task LSTM model to predict 20 water quality variables simultaneously. Unlike single-task models that require training separate models for each target variable [32, 53, 57], the multi-task approach leverages shared learning of hidden relationships among variables, improving predictive performance, and reducing computational costs, which is critical for modeling complex biogeochemical processes [23].

We trained the LSTM model using PyTorch, with a two-layer architecture, 512 hidden units, and a dropout rate of 0.3. The input sequence length was set to 365 days [23], which corresponds to one full year of data. This length was chosen to capture seasonal patterns and annual cycles, which are essential in domains like climate data where yearly trends are significant. The minibatch size was 512. The training was conducted for 300 epochs using the AdamW optimizer with an initial learning rate of 0.001 and a decay rate of 0.5 applied every 100 epochs. The mean squared error (MSE) between model predictions and normalized ground truths was used as the loss function for backpropagation. All experiments were performed on NVIDIA RTX 3090 GPUs.

The model evaluation followed a robust temporal holdout strategy, ensuring the statistical representativeness of the training data while accounting for climate variability [58]. Following the approach of [23], data from four out of every five years were used for training, with the remaining year in each five-year period used for testing. Specifically, observations from the years 1985, 1990, 1995, 2000, 2005, 2010, and 2015 were systematically withheld during training and used exclusively for testing.

To prepare the input data for the LSTM model, we applied different normalization techniques based on the distribution of each variable. For vegetation indices, water quality station coordinates, time-related variables, and the target water quality variables temperature, DO, and pH, we used min-max normalization. This method effectively scales variables within a range of 0 to 1, preserving the relative differences between values. For other input features and target water quality variables, we employed a log-min-max normalization strategy, which combines logarithmic transformation and min-max scaling. This approach was particularly effective for handling variables with skewed distributions. Normalization parameters (minimum and maximum values) were calculated exclusively from the training data. During testing, the same parameters were applied to

normalize the test data. This ensures consistency between the training and testing phases, avoids information leakage from the test dataset to the training process, and allows for fair model evaluation on the same scale as the training data.

The Kling-Gupta Efficiency (KGE, Eq. (1)) [59] was selected as the primary metric to evaluate model performance for each of the 482 basins. KGE is widely used in hydrological modeling studies [23, 60, 61]. It ranges from $-\infty$ to 1, where a value of 1 indicates perfect agreement, and values below -0.41 denote poor performance, where predictions are worse than the mean of observations [62]. KGE is mathematically defined as:

$$\text{KGE} = 1 - \sqrt{(r - 1)^2 + (\beta - 1)^2 + (\gamma - 1)^2}, \quad (1)$$

where r represents the correlation coefficient between observations (O) and model predictions (P); $\beta = \mu_P/\mu_O$ is the bias ratio, defined as the ratio of the mean of predictions (μ_P) to the mean of observations (μ_O); and $\gamma = \sigma_P/\sigma_O$ is the variability ratio, defined as the ratio of the standard deviation of predictions (σ_P) to the standard deviation of observations (σ_O). Note that metrics were computed using the original data, with inverse normalization applied to model outputs.

Trustworthiness evaluation framework

Outliers simulation. Extreme high and low values in water quality datasets are not uncommon due to a combination of factors, including sensor malfunctions, instrument detection limits, episodic pollution events (e.g., storm-driven contaminant pulses), and anthropogenic influences such as industrial discharges or agricultural runoff. Additionally, natural processes like sediment resuspension, extreme weather conditions, and seasonal fluctuations can drive sudden shifts in the concentration of water quality variables, further contributing to the presence of outliers in observational datasets. To evaluate the model's robustness against such anomalies, we introduced artificial outliers into the training data by modifying 10% of the data points. This proportion was chosen to strike a balance between realism and analytical rigor: it represents scenarios where outliers could meaningfully impact model predictions while preserving the dataset's overall structure and distribution. The 10% threshold aligns with common practices in outlier analysis, where similar proportions are often used to evaluate model sensitivity to rare events [63].

To generate high-value outliers, we increased 10% of non-maximum values to become the upper extreme of their respective distributions. Similarly, low-value outliers were created by decreasing 10% of non-minimum values to become the lower extreme. These perturbations were applied independently to input features and target water quality variables, enabling a comprehensive evaluation of the model's resilience to anomalous data points. To quantify the impact of these outliers, we computed the average KGE across all scenarios and

evaluated performance degradation by calculating the percentage difference relative to the baseline performance.

Random measurement noise simulation. In environmental monitoring, measurement errors are inevitable due to sensor inaccuracies, environmental variability, and sample collection inconsistencies. Assessing the impact of such noise, or uncertainty, in model input data on model performance is a component of our evaluation of model trustworthiness. To systematically assess this impact, we introduced controlled random perturbations into the training data to simulate realistic noise conditions. Noise was applied to 30% and 40% of the dataset, applied either to input features or target variables. For input features, additive deviations were introduced to mimic common sources of error. For target variables, proportional random modifications were applied to reflect discrepancies in observed water quality values, which can occur due to sampling inconsistencies, laboratory measurement precision limits, or data logging errors. To capture varying degrees of random noise, the noise magnitude was set at 40% and 50%. The average KGE across all noise scenarios was computed, and performance degradation was assessed by calculating the percentage difference relative to the baseline LSTM model performance.

Adversarial inputs generation. Adversarial vulnerabilities are a well-documented issue in AI models [14, 64] and can have significant consequences in environmental modeling [58]. In water quality applications, adversarially perturbed inputs could arise from systematic errors in sensor readings, cyber-physical security threats in IoT-based monitoring networks, or targeted manipulation of data used in regulatory decision-making [65].

In this work, we used the Projected Gradient Descent (PGD) method [66] to introduce adversarial perturbations to input features for evaluating the LSTM model’s robustness. Unlike random noise or outliers, which are typically random or extreme deviations from the data distribution, adversarial perturbations are carefully crafted to exploit specific vulnerabilities in the model, often targeting the decisions that the model has learned. Specifically, PGD initializes a slight random perturbation, then adjusts the input each iteration to maximize the model’s loss function while staying within set bounds to remain both undetected and effective.

To systematically assess model vulnerability, adversarial noise was applied to 10% and 20% of the dataset. Two attack budgets (0.05 and 0.1) were employed, specifying the maximum allowed perturbation magnitude for each adversarial sample. A step size of one-quarter of the attack budget was used per iteration to ensure gradual, controlled modifications and optimize adversarial effectiveness. The model’s average performance was computed across all test scenarios, and the performance degradation was quantified as the percentage difference in KGE values relative to the baseline model.

Predictive uncertainty quantification. To evaluate the uncertainty in the water quality predictions by the LSTM model, we employed Monte Carlo (MC) dropout [22], a method that introduces stochasticity during inference to estimate predictive uncertainty. Specifically, during model inference, a dropout probability of 0.3 was applied, which randomly deactivates a proportion of the model’s units. This process was repeated 50 times, with each forward pass producing a slightly different set of predictions due to the stochastic nature of the dropout. The uncertainty in the model’s predictions was quantified by calculating the standard deviation of the KGE values across the 50 ensemble predictions. This approach provides a robust and interpretable measure of the model’s confidence [22], helping identify variables where predictions may be less reliable.

Feature importance analysis. We employed a systematic framework that combines ablation studies with a traverse approach to evaluate the contributions of five input categories: meteorological forcing (M), runoff (Q), rainfall chemistry (RC), vegetation indices (V), and static basin attributes (BA), to model performance. Across all experiments, spatial variables (e.g., latitude and longitude) and temporal variables (e.g., datenum, sinT, and cosT) were consistently included as baseline predictors, providing essential spatial and temporal context.

Ablation studies are commonly used to assess feature importance in hydrology and water quality modeling [32, 67, 68]. Here, the importance of each feature category is quantified by the reduction in model performance (e.g., Kling–Gupta Efficiency, KGE) when that category is removed from the full model. This approach quantifies how much additional contribution a given feature category brings to a predictive model beyond what other features already contribute.

In the traverse approach, we assessed model performance across all possible combinations of the five input categories, resulting in 32 unique model configurations. This design provides a more detailed analysis of each category’s contribution by examining both its individual effects and its interactions with other input categories. To quantify feature importance, we computed the average performance reduction between subsets that include a given category and those that exclude it, thus capturing both direct and marginal contributions to overall model performance.

Generalization to unseen basins. To test the model’s generalizability, we employed a spatial holdout strategy in which 80% of the basins were randomly selected for training and the remaining 20% were for testing. This ensures that the test basins are completely unseen during training, allowing us to evaluate the model’s ability to generalize to new geographic regions characterized by distinct geographic, climatic, and hydrological conditions.

Data sources

Streamflow and water quality data were extracted from the U.S. Geological Survey (USGS) National Water Information System (NWIS) database (<https://waterdata.usgs.gov/nwis>). Meteorological variables were extracted from the gridMET dataset (<https://www.climatologylab.org/gridmet.html>). Vegetation indices were acquired from the Global Land Surface Satellite (GLASS) dataset (<http://www.glass.umd.edu/Download.html>). Rainfall chemistry data were retrieved from the National Atmospheric Deposition Program/National Trends Network (NADP/NTN) (<https://nadp.slh.wisc.edu/networks/national-trends-network/>). Basin attributes were obtained from the Geospatial Attributes of Gages for Evaluating Streamflow, version II (GAGES-II) database (<https://www.sciencebase.gov/catalog/item/631405bbd34e36012efa304a>). Processed data for the 482 basins used in this study are publicly available at <https://figshare.com/s/e0151c12b6e6482bae83>.

Code and data availability

Python scripts for downloading raw data are available at: <https://github.com/fkwai/geolearn/tree/master/hydroDL/data>. The LSTM modeling code developed in this study is provided in the supplementary file. Python (3.8.18) codes for statistical analysis and plotting are available from the authors upon request.

Acknowledgements

Xiaobo Xia was supported by MoE Key Laboratory of Brain-inspired Intelligent Perception and Cognition, University of Science and Technology of China (Grant No. 2421002). Xiaofeng Liu was supported by Schmidt Sciences, LLC. Tongliang Liu was partially supported by the following Australian Research Council projects: FT220100318, DP220102121, LP220100527, LP220200949, and IC190100031.

References

- [1] Dudgeon, D. *et al.* Freshwater biodiversity: importance, threats, status and conservation challenges. *Biological Reviews* **81**, 163–182 (2006).
- [2] McKeown, A. E. *Impact of water pollution on human health and environmental sustainability* (IGI Global, 2015).
- [3] du Plessis, A. Persistent degradation: Global water quality challenges and required actions. *One Earth* **5**, 129–131 (2022).

- [4] Keiser, D. A., Kling, C. L. & Shapiro, J. S. The low but uncertain measured benefits of us water quality policy. *Proceedings of the National Academy of Sciences* **116**, 5262–5269 (2019).
- [5] Liu, X. & Georgakakos, A. P. Chlorophyll a estimation in lakes using multi-parameter sonde data. *Water Research* **205**, 117661 (2021).
- [6] Babatunde, A. A study on traditional water quality assessment methods. *Risk Assessment and Management Decisions* **1**, 41–52 (2024).
- [7] Nearing, G. *et al.* Global prediction of extreme floods in ungauged watersheds. *Nature* **627**, 559–563 (2024).
- [8] Kratzert, F. *et al.* Toward improved predictions in ungauged basins: Exploiting the power of machine learning. *Water Resources Research* **55**, 11344–11354 (2019).
- [9] Shen, C. A transdisciplinary review of deep learning research and its relevance for water resources scientists. *Water Resources Research* **54**, 8558–8593 (2018).
- [10] Rudin, C. Stop explaining black box machine learning models for high stakes decisions and use interpretable models instead. *Nature Machine Intelligence* **1**, 206–215 (2019).
- [11] Li, B. *et al.* Trustworthy ai: From principles to practices. *ACM Computing Surveys* **55**, 1–46 (2023).
- [12] Liang, W. *et al.* Advances, challenges and opportunities in creating data for trustworthy ai. *Nature Machine Intelligence* **4**, 669–677 (2022).
- [13] Eshete, B. Making machine learning trustworthy. *Science* **373**, 743–744 (2021).
- [14] Kurakin, A., Goodfellow, I. J. & Bengio, S. Adversarial examples in the physical world. In *Artificial Intelligence Safety and Security*, 99–112 (2018).
- [15] Tomsett, R. *et al.* Rapid trust calibration through interpretable and uncertainty-aware ai. *Patterns* **1** (2020).
- [16] Zhu, M., Zhang, H., Jiao, A., Karniadakis, G. E. & Lu, L. Reliable extrapolation of deep neural operators informed by physics or sparse observations. *Computer Methods in Applied Mechanics and Engineering* **412**, 116064 (2023).
- [17] Markus, A. F., Kors, J. A. & Rijnbeek, P. R. The role of explainability in creating trustworthy artificial intelligence for health care: a comprehensive survey of the terminology, design choices, and evaluation strategies. *Journal of Biomedical Informatics* **113**, 103655 (2021).
- [18] Fernández Llorca, D. & Gómez, E. Trustworthy autonomous vehicles. *Publications Office of the European Union, Luxembourg*, EUR **30942** (2021).
- [19] Wang, X. *et al.* Sentiment analysis via trustworthy label enhancement for consumer electronics applications. *IEEE Transactions on Consumer Electronics* (2024).

[20] McGovern, A. *et al.* The value of convergence research for developing trustworthy ai for weather, climate, and ocean hazards. *npj Natural Hazards* **1**, 13 (2024).

[21] Zhi, W., Appling, A. P., Golden, H. E., Podgorski, J. & Li, L. Deep learning for water quality. *Nature water* **2**, 228–241 (2024).

[22] Gal, Y. & Ghahramani, Z. Dropout as a bayesian approximation: Representing model uncertainty in deep learning. In *International Conference on Machine Learning*, 1050–1059 (2016).

[23] Fang, K., Caers, J. & Maher, K. Modeling continental us stream water quality using long-short term memory and weighted regressions on time, discharge, and season. *Frontiers in Water* **6**, 1456647 (2024).

[24] Saha, G. K., Rahmani, F., Shen, C., Li, L. & Cibin, R. A deep learning-based novel approach to generate continuous daily stream nitrate concentration for nitrate data-sparse watersheds. *Science of the Total Environment* **878**, 162930 (2023).

[25] Bai, T., Luo, J., Zhao, J., Wen, B. & Wang, Q. Recent advances in adversarial training for adversarial robustness. *arXiv preprint arXiv:2102.01356* (2021).

[26] Lin, F., Fang, X. & Gao, Z. Distributionally robust optimization: A review on theory and applications. *Numerical Algebra, Control and Optimization* **12**, 159–212 (2022).

[27] Vaswani, A. *et al.* Attention is all you need. *Advances in Neural Information Processing Systems* **30** (2017).

[28] Hu, Y. & Khan, L. Uncertainty-aware reliable text classification. In *Proceedings of the 27th ACM SIGKDD Conference on Knowledge Discovery & Data Mining*, 628–636 (2021).

[29] Einbinder, B.-S., Romano, Y., Sesia, M. & Zhou, Y. Training uncertainty-aware classifiers with conformalized deep learning. *Advances in Neural Information Processing Systems* **35**, 22380–22395 (2022).

[30] Li, W., Huang, X., Lu, J., Feng, J. & Zhou, J. Learning probabilistic ordinal embeddings for uncertainty-aware regression. In *Proceedings of the IEEE/CVF Conference on Computer Vision and Pattern Recognition*, 13896–13905 (2021).

[31] Chua, M. *et al.* Tackling prediction uncertainty in machine learning for healthcare. *Nature Biomedical Engineering* **7**, 711–718 (2023).

[32] Zhi, W., Klingler, C., Liu, J. & Li, L. Widespread deoxygenation in warming rivers. *Nature Climate Change* **13**, 1105–1113 (2023).

[33] Wang, S., Peng, H., Hu, Q. & Jiang, M. Analysis of runoff generation driving factors based on hydrological model and interpretable machine learning method. *Journal of Hydrology: Regional Studies* **42**, 101139 (2022).

- [34] Yang, D. *et al.* Predictor selection for cnn-based statistical downscaling of monthly precipitation. *Advances in Atmospheric Sciences* **40**, 1117–1131 (2023).
- [35] Hooker, S., Erhan, D., Kindermans, P.-J. & Kim, B. A benchmark for interpretability methods in deep neural networks. *Advances in Neural Information Processing Systems* **32** (2019).
- [36] Catay, A. *et al.* Marginal contribution feature importance—an axiomatic approach for explaining data. In *International Conference on Machine Learning*, 1324–1335 (2021).
- [37] Lundberg, S. M. & Lee, S.-I. A unified approach to interpreting model predictions. *Advances in Neural Information Processing Systems* **30** (2017).
- [38] Sundararajan, M., Taly, A. & Yan, Q. Axiomatic attribution for deep networks. In *International Conference on Machine Learning*, 3319–3328 (PMLR, 2017).
- [39] Li, W. *et al.* Research progress in water quality prediction based on deep learning technology: a review. *Environmental Science and Pollution Research* **31**, 26415–26431 (2024).
- [40] Calvin, K. *et al.* Ipcc, 2023: Climate change 2023: Synthesis report, summary for policymakers. contribution of working groups i, ii and iii to the sixth assessment report of the intergovernmental panel on climate change [core writing team, h. lee and j. romero (eds.)]. ipcc, geneva, switzerland. *IPCC, 2023: Climate Change 2023: Synthesis Report. Contribution of Working Groups I, II and III to the Sixth Assessment Report of the Intergovernmental Panel on Climate Change [Core Writing Team, H. Lee and J. Romero (eds.)]. IPCC, Geneva, Switzerland.* 1–34 (2023).
- [41] Agrawal, T., Goodwell, A. & Kumar, P. Improving stream solute predictions with a modified lstm model incorporating solute interdependences and hysteresis patterns. *Journal of Geophysical Research: Machine Learning and Computation* **2**, e2024JH000383 (2025).
- [42] Daw, A., Karpatne, A., Watkins, W. D., Read, J. S. & Kumar, V. Physics-guided neural networks (pgnn): An application in lake temperature modeling. In *Knowledge Guided Machine Learning*, 353–372 (2022).
- [43] Bhasme, P., Vagadiya, J. & Bhatia, U. Enhancing predictive skills in physically-consistent way: Physics informed machine learning for hydrological processes. *Journal of Hydrology* **615**, 128618 (2022).
- [44] Daneker, M. *et al.* Transfer learning on physics-informed neural networks for tracking the hemodynamics in the evolving false lumen of dissected aorta. *Nexus* **1** (2024).
- [45] Wang, S., Wang, H. & Perdikaris, P. Learning the solution operator of parametric partial differential equations with physics-informed deepnets. *Science Advances* **7**, eabi8605 (2021).
- [46] Brown, T. *et al.* Language models are few-shot learners. *Advances in Neural Information Processing Systems* **33**, 1877–1901 (2020).

[47] Gundersen, O. E., Gil, Y. & Aha, D. W. On reproducible ai: Towards reproducible research, open science, and digital scholarship in ai publications. *AI Magazine* **39**, 56–68 (2018).

[48] U.S. Geological Survey. National Water Information System (2025). Available at: <https://waterdata.usgs.gov/nwis> (Last accessed: March 5, 2025).

[49] Falcone, J. A. Gages-ii: Geospatial attributes of gages for evaluating streamflow. *USGS Report* **41** (2011).

[50] Abatzoglou, J. T. Development of gridded surface meteorological data for ecological applications and modelling. *International Journal of Climatology* **33**, 121–131 (2013).

[51] Liang, S. *et al.* A long-term global land surface satellite (glass) data-set for environmental studies. *International Journal of Digital Earth* **6**, 5–33 (2013).

[52] National Atmospheric Deposition Program (NADP). National Trends Network. <http://nadp.slu.wisc.edu/networks/national-trends-network/> (2005). Last accessed: January 16, 2025.

[53] Zhi, W. *et al.* Increasing phosphorus loss despite widespread concentration decline in us rivers. *Proceedings of the National Academy of Sciences* **121**, e2402028121 (2024).

[54] Spahr, N. E., Dubrovsky, N. M., Gronberg, J. M., Franke, O. L. & Wolock, D. M. Nitrate loads and concentrations in surface-water base flow and shallow groundwater for selected basins in the united states, water years 1990-2006. Tech. Rep., US Geological Survey (2010).

[55] Hochreiter, S. & Schmidhuber, J. Long short-term memory. *Neural computation* **9**, 1735–1780 (1997).

[56] Noh, S.-H. Analysis of gradient vanishing of rnns and performance comparison. *Information* **12**, 442 (2021).

[57] Yao, J., Chen, S. & Ruan, X. Interpretable ceemdan-fe-lstm-transformer hybrid model for predicting total phosphorus concentrations in surface water. *Journal of Hydrology* **629**, 130609 (2024).

[58] McGovern, A., Ebert-Uphoff, I., Gagne II, D. J. & Bostrom, A. Why we need to focus on developing ethical, responsible, and trustworthy artificial intelligence approaches for environmental science. *Environmental Data Science* **1**, e6 (2022).

[59] Gupta, H. V., Kling, H., Yilmaz, K. K. & Martinez, G. F. Decomposition of the mean squared error and nse performance criteria: Implications for improving hydrological modelling. *Journal of Hydrology* **377**, 80–91 (2009).

[60] Hunt, K. M., Matthews, G. R., Pappenberger, F. & Prudhomme, C. Using a long short-term memory (lstm) neural network to boost river streamflow forecasts over the western united states. *Hydrology and Earth System Sciences* **26**, 5449–5472 (2022).

- [61] He, M., Wu, S., Huang, B., Kang, C. & Gui, F. Prediction of total nitrogen and phosphorus in surface water by deep learning methods based on multi-scale feature extraction. *Water* **14**, 1643 (2022).
- [62] Knoben, W. J., Freer, J. E. & Woods, R. A. Inherent benchmark or not? comparing nash–sutcliffe and kling–gupta efficiency scores. *Hydrology and Earth System Sciences* **23**, 4323–4331 (2019).
- [63] Oyeyemi, G. M., Bukoye, A. & Akeyede, I. Comparison of outlier detection procedures in multiple linear regressions. *American Journal of Mathematics and Statistics* **5**, 37–41 (2015).
- [64] Finlayson, S. G. *et al.* Adversarial attacks on medical machine learning. *Science* **363**, 1287–1289 (2019).
- [65] Wu, Y. Robust learning-enabled intelligence for the internet of things: A survey from the perspectives of noisy data and adversarial examples. *IEEE Internet of Things Journal* **8**, 9568–9579 (2020).
- [66] Madry, A., Makelov, A., Schmidt, L., Tsipras, D. & Vladu, A. Towards deep learning models resistant to adversarial attacks. *arXiv preprint arXiv:1706.06083* (2017).
- [67] Li, K., Huang, G. & Baetz, B. Development of a wilks feature importance method with improved variable rankings for supporting hydrological inference and modelling. *Hydrology and Earth System Sciences* **25**, 4947–4966 (2021).
- [68] Dvorett, D., Davis, C. & Papeş, M. Mapping and hydrologic attribution of temporary wetlands using recurrent landsat imagery. *Wetlands* **36**, 431–443 (2016).

Table of content

Supplementary figures

- **Fig. S1.** Spatial distribution of studied basins classified by land uses. Following the USGS classification criteria [54], agricultural basins (AG, red) are defined as having more than 50% agricultural land (PLANTNLCD06 in the GAGES-II database) and at most 5% urban land (DEVNLCD06). Undeveloped basins (UD, green) have at most 5% urban land and at most 25% agricultural land. Urban basins (UR, purple) are defined as having more than 25% urban land and at most 25% agricultural land, while mixed basins (MX, yellow) include all other combinations of urban, agricultural, and undeveloped land. Among the selected basins, 3.1% were classified as AG, 11.2% as UR, 35.1% as UD, and 50.6% as MX.
- **Fig. S2.** Multi-task LSTM model performances across undeveloped basins (UD), urban basins (UR), mixed basins (MX), and agricultural basins (AG), are shown as the cumulative distribution function (CDF) of the KGE. Curves that remain lower demonstrate better performance.
- **Fig. S3.** Water quality data coverage (%) across basins of different land use types, computed as the ratio of days monitored to the total number of days between 01/01/1982 and 12/31/2018. A coverage of 100% indicates that water quality measurements were available for the entire study period and 0% indicates no measurements were available. The boxplots display the median (central line), interquartile range (IQR, represented by the boxes spanning the first (Q1) to the third quartile (Q3)), and whiskers extending to $Q1 - 1.5 \times IQR$ and $Q3 + 1.5 \times IQR$.
- **Fig. S4.** Simplicity index distributions across undeveloped basins (UD), urban basins (UR), mixed basins (MX), and agricultural basins (AG). The simplicity index (adapted from [23]) quantifies the proportion of variance in water quality dynamics explained by linear relationships with runoff and annual cycles. Lower CDF (cumulative distribution function) curves indicate higher simplicity.
- **Fig. S5.** Context-dependent feature importance (KGE reduction) of meteorological variables (M) and runoff (Q) derived via the Traverse method. Dark blue boxplots represent KGE reduction from excluding Q when M is already excluded, whereas light blue boxplots represent excluding Q when M is included. Similarly, dark red boxplots show the KGE reduction from excluding M when Q is absent, whereas light red boxplots represent excluding M when Q is included. Wilcoxon signed-rank tests were conducted to assess whether median KGE reductions from subsets lacking Q or M were significantly greater than those from subsets where Q or M were present (** $p < 0.001$). The results indicate that meteorological variables become largely redundant when runoff is included.

- **Fig. S6.** Boxplot of Kling-Gupta Efficiency (KGE) values for the testing basins under a random spatial training-testing split, evaluated across 20 predicted water quality variables associated with physical/chemical properties, geochemical weathering processes, and nutrient cycling, respectively. Each boxplot shows the median (central line), interquartile range (IQR, represented by the boxes spanning the first (Q1) to the third quartile (Q3)), and whiskers extending to $Q1 - 1.5 \times IQR$ and $Q3 + 1.5 \times IQR$. The number labeled on the box indicates the median.

Supplementary tables

- **Table S1.** Summary of the studied water quality variables and the average number of observations per basin, based on 482 U.S. rivers between 01/01/1982 and 12/31/2018.
- **Table S2.** Model input features, consisting of 25 time series variables and 49 static basin attributes (sourced from the GAGES-II database).

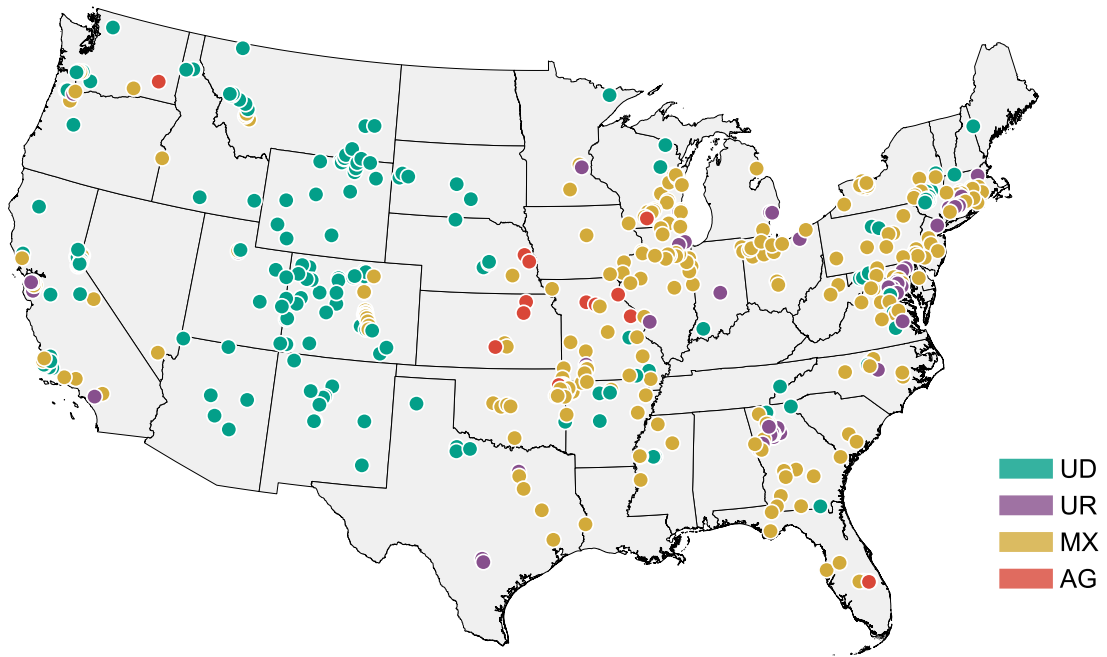


Fig. S1. Spatial distribution of studied basins classified by land uses. Following the USGS classification criteria [54], agricultural basins (AG, red) are defined as having more than 50% agricultural land (PLANTNLCD06 in the GAGES-II database) and at most 5% urban land (DEVNLCD06). Undeveloped basins (UD, green) have at most 5% urban land and at most 25% agricultural land. Urban basins (UR, purple) are defined as having more than 25% urban land and at most 25% agricultural land, while mixed basins (MX, yellow) include all other combinations of urban, agricultural, and undeveloped land. Among the selected basins, 3.1% were classified as AG, 11.2% as UR, 35.1% as UD, and 50.6% as MX.

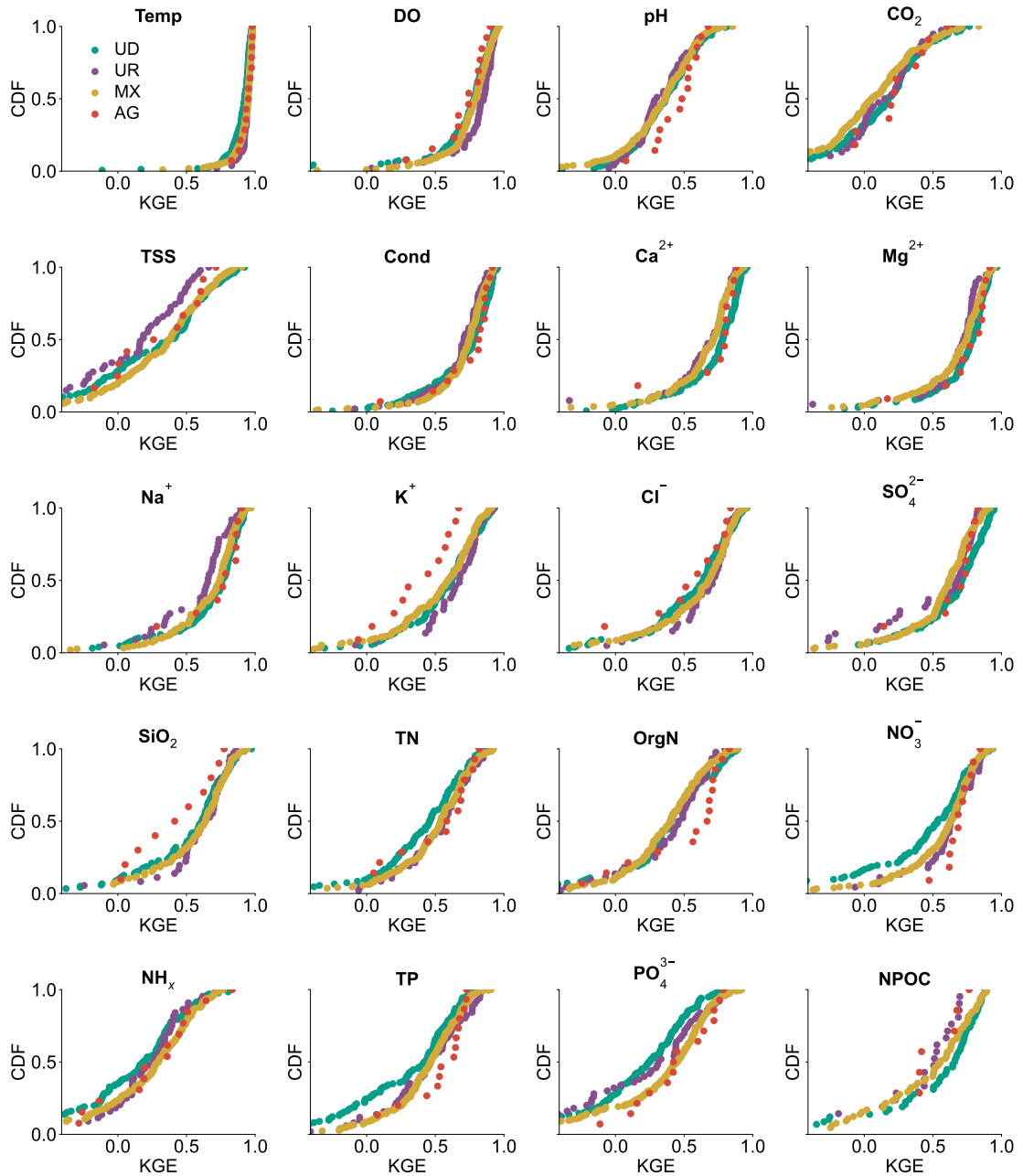


Fig. S2. Multi-task LSTM model performances across undeveloped basins (UD), urban basins (UR), mixed basins (MX), and agricultural basins (AG), are shown as the cumulative distribution function (CDF) of the KGE. Curves that remain lower demonstrate better performance.

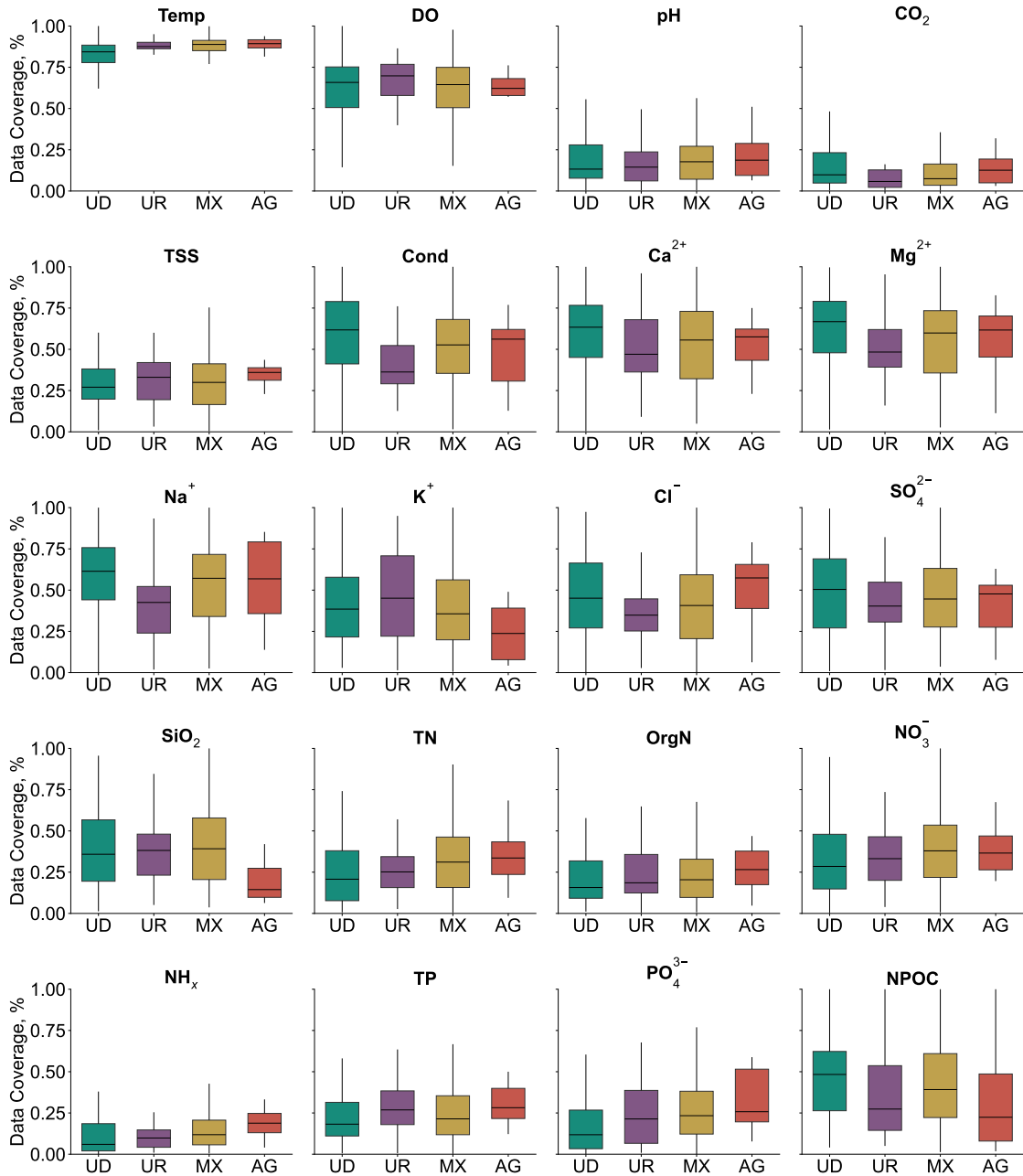


Fig. S3. Water quality data coverage (%) across basins of different land use types, computed as the ratio of days monitored to the total number of days between 01/01/1982 and 12/31/2018. A coverage of 100% indicates that water quality measurements were available for the entire study period and 0% indicates no measurements were available. The boxplots display the median (central line), interquartile range (IQR, represented by the boxes spanning the first (Q1) to the third quartile (Q3)), and whiskers extending to $Q1 - 1.5 \times IQR$ and $Q3 + 1.5 \times IQR$.

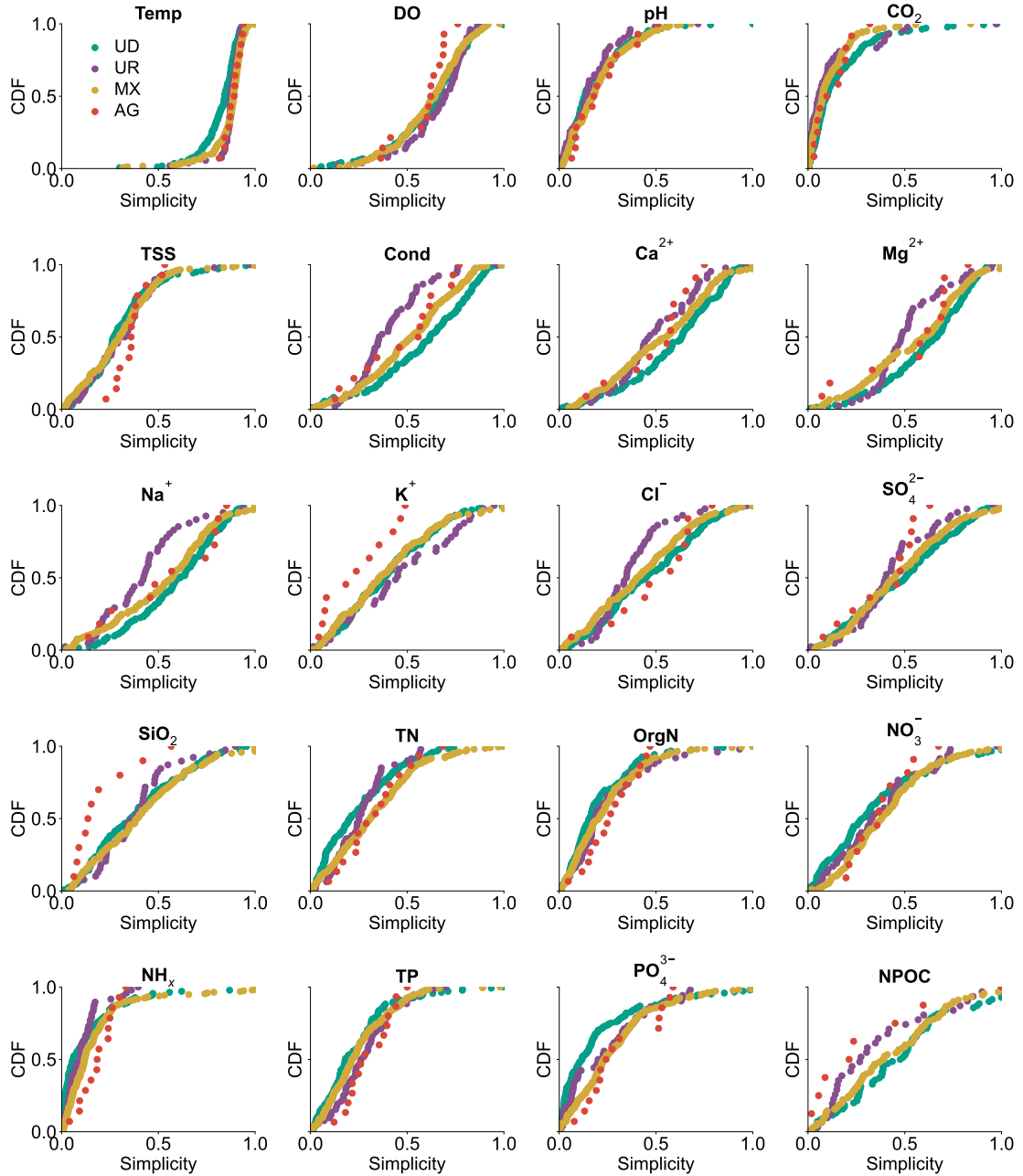


Fig. S4. Simplicity index distributions across undeveloped basins (UD), urban basins (UR), mixed basins (MX), and agricultural basins (AG). The simplicity index (adapted from [23]) quantifies the proportion of variance in water quality dynamics explained by linear relationships with runoff and annual cycles. Lower CDF (cumulative distribution function) curves indicate higher simplicity.

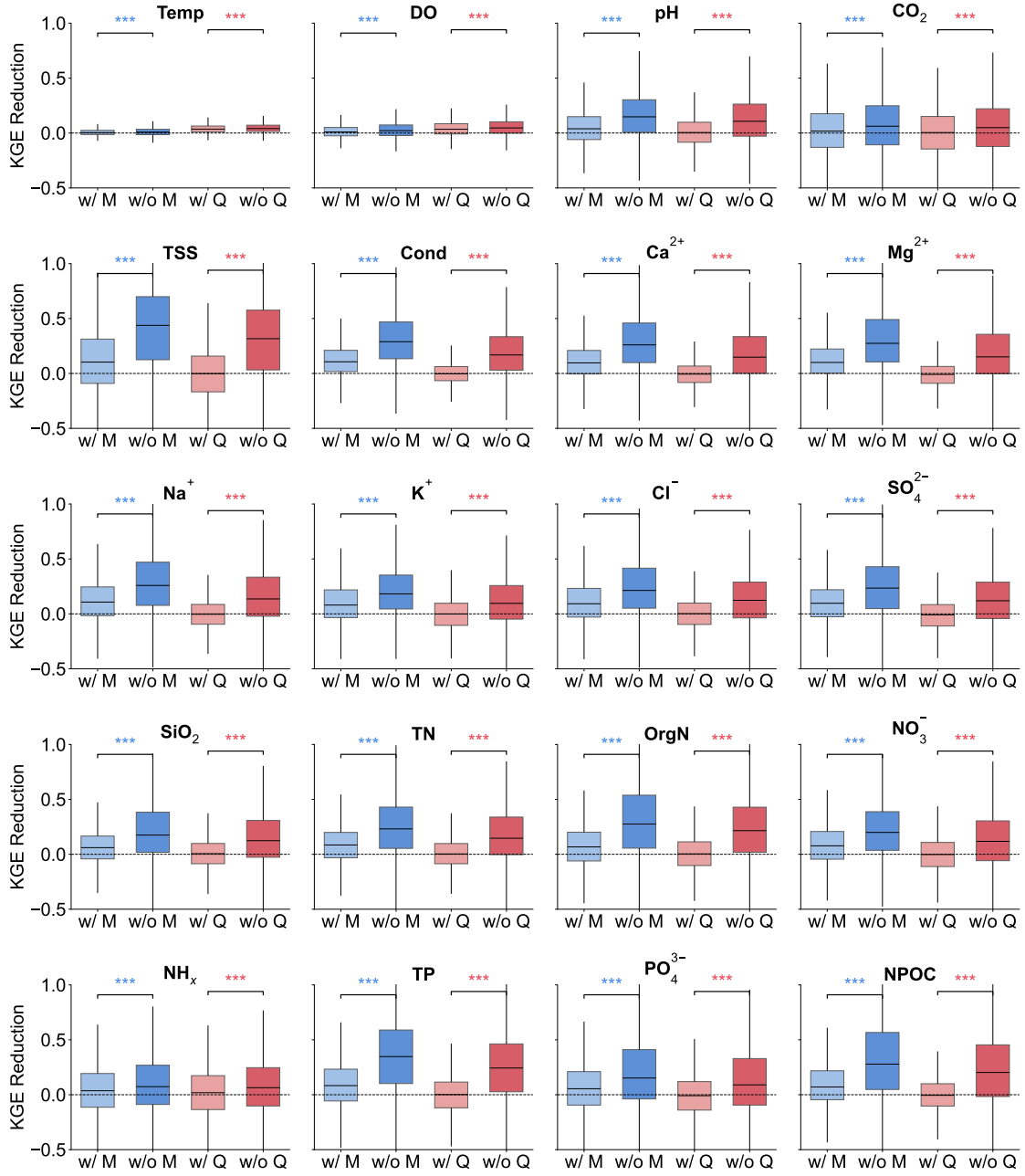


Fig. S5. Context-dependent feature importance (KGE reduction) of meteorological variables (M) and runoff (Q) derived via the Traverse method. Dark blue boxplots represent KGE reduction from excluding Q when M is already excluded, whereas light blue boxplots represent excluding Q when M is included. Similarly, dark red boxplots show the KGE reduction from excluding M when Q is absent, whereas light red boxplots represent excluding M when Q is included. Wilcoxon signed-rank tests were conducted to assess whether median KGE reductions from subsets lacking Q or M were significantly greater than those from subsets where Q or M were present (***($p < 0.001$). The results indicate that meteorological variables become largely redundant when runoff is included.

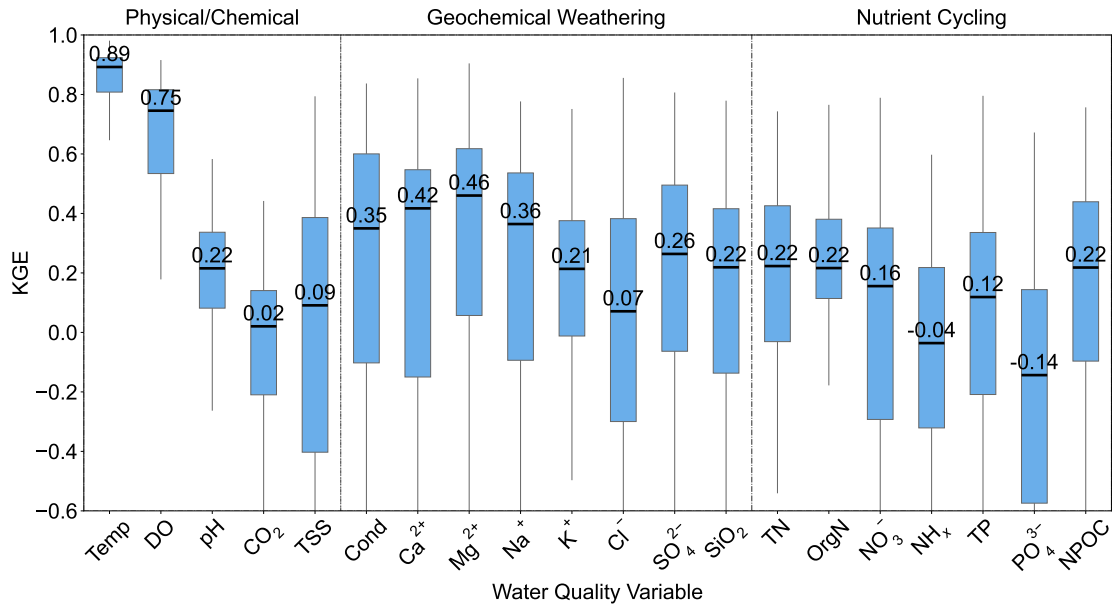


Fig. S6. Boxplot of Kling-Gupta Efficiency (KGE) values for the testing basins under a random spatial training-testing split, evaluated across 20 predicted water quality variables associated with physical/chemical properties, geochemical weathering processes, and nutrient cycling, respectively. Each boxplot shows the median (central line), interquartile range (IQR, represented by the boxes spanning the first (Q1) to the third quartile (Q3)), and whiskers extending to $Q1 - 1.5 \times IQR$ and $Q3 + 1.5 \times IQR$. The number labeled on the box indicates the median.

Table S1. Summary of the studied water quality variables and the average number of observations per basin, based on 482 U.S. rivers between 01/01/1982 and 12/31/2018.

USGS code	Description	Abbreviation	Unit	# Observations per basin
00010	Water temperature	Temp	°C	330.5
00095	Specific conductance	Cond	uS/cm at 25°C	285.6
00300	Oxygen	DO	mg/L	197.8
00400	pH	pH	-	224.9
00405	Carbon dioxide	CO ₂	mg/L	129.2
00600	Total nitrogen	TN	mg/L	193.3
00605	Organic nitrogen	OrgN	mg/L	171.7
00618	Nitrate	NO ₃ ⁻	mg/L as N	138.3
00660	Orthophosphate	PO ₄ ³⁻	mg/L as PO ₄ ³⁻	204.9
00665	Total phosphorus	TP	mg/L as P	266.9
00681	Organic carbon	NPOC	mg/L	60.3
00915	Calcium	Ca ²⁺	mg/L	131.7
00925	Magnesium	Mg ²⁺	mg/L	131.8
00930	Sodium	Na ⁺	mg/L	117.3
00935	Potassium	K ⁺	mg/L	114.8
00940	Chloride	Cl ⁻	mg/L	184.1
00945	Sulfate	SO ₄ ²⁻	mg/L	154.3
00955	Silica	SiO ₂	mg/L	116.1
71846	Ammonia and ammonium	NH _x (NH ₃ and NH ₄ ⁺)	mg/L as NH ₄ ⁺	184.1
80154	Suspended sediment concentration	TSS	mg/L	305.4

Table S2. Model input features, consisting of 25 time series variables and 49 static basin attributes (sourced from the GAGES-II database).

Group	Name	Type	Description	Unit
Runoff	runoff	time-varying	Area normalized streamflow from USGS	m/y
Meteorological forcings	pr	time-varying	Daily total precipitation	mm/day
	sph	time-varying	Specific humidity	unitless
	srad	time-varying	Surface downwelling solar radiation	W/m ²
	tmmn	time-varying	Daily minimum 2-meter air temperature	F
	tmmx	time-varying	Daily maximum 2-meter air temperature	F
	pet	time-varying	Reference grass evapotranspiration	mm/day
Rainfall chemistry	etr	time-varying	Reference alfalfa evapotranspiration	mm/day
	pH	time-varying	Logarithm of the H ion activity	unitless
	Cond	time-varying	Electrical conductivity of water	µS/cm
	Ca ²⁺	time-varying	Ca ion concentration	mg/L
	Mg ²⁺	time-varying	Mg ion concentration	mg/L
	K ⁺	time-varying	K ion concentration	mg/L
	Na ⁺	time-varying	Na ion concentration	mg/L
	NH ₄	time-varying	NH ₄ concentration	mg/L
	NO ₃	time-varying	NO ₃ concentration	mg/L
	Cl ⁻	time-varying	Cl ion concentration	mg/L
	SO ₄	time-varying	SO ₄ concentration	mg/L
	distNTN	time-varying	The distance to the nearest NTN sampling site	km
Vegetation indices	LAI	time-varying	Leaf area index of vegetation	m ² /m ²
	FAPAR	time-varying	Fraction of absorbed photosynthetically active radiation	unitless
	NPP	time-varying	Net primary production	gC/m ² /day
Time variables	datenum	time-varying	The number of days relative to January 1, 2000	unitless
	sinT	time-varying	Sine of datenum	unitless
	cosT	time-varying	Cosine of datenum	unitless
Basic characteristics	HYDRO_DISTURB_INDX	static	Hydrologic “disturbance index” score, based on 7 variables: 1) MAJ_DDENS_2009, 2) WATER_WITHDR, 3) change in dam storage 1950-2009, 4) CANALS_PCT, 5) RAW_DIS_NEAREST_MAJ_NPDES, 6) ROADS_KM_SQ_KM, and 7) FRAGUN_BASIN	unitless
	BAS_COMPACTNESS	static	Watershed compactness ratio, = area/perimeter ² * 100; higher number = more compact shape	unitless
	DRAIN_SQKM	static	Watershed drainage area, sq km, as delineated in our basin boundary	km ²
Geology	GEOL_REEDBUSH_DOM	static	Dominant (highest percent of area) geology, derived from a simplified version of Reed & Bush (2001) - Generalized Geologic Map of the Conterminous United States	unitless
	GEOL_REEDBUSH_DOM_PCT	static	Percentage of the watershed covered by the dominant geology type	percentage
Hydrologic characteristics	STREAMS_K_S_KM	static	Stream density, km of streams per watershed sq km, from NHD 100k streams	km/km ²
	STRAHLER_MAX	static	Maximum Strahler stream order in the watershed, from NHDPlus	unitless
	MAINSTEM_SINUOSITY	static	Sinuosity of mainstem stream line, from our delineation of mainstem stream lines. Defined as curvilinear length of the mainstem stream line divided by the straight-line distance between the end points of the line.	unitless
	BFI_AVE	static	Base Flow Index (BFI). The BFI is a ratio of base flow to total streamflow, expressed as a percentage and ranging from 0 to 100. Base flow is the sustained, slowly varying component of streamflow, usually attributed to ground-water discharge to a stream.	percentage
	CONTACT	static	Subsurface flow contact time index	days
	PCT_1ST_ORDER	static	Percent of stream lengths in the watershed which are first-order streams (Strahler order); from NHDPlus & percentage	percentage
	PCT_2ND_ORDER	static	Percent of stream lengths in the watershed which are second-order streams (Strahler order); from NHDPlus & percentage	percentage
	PCT_3RD_ORDER	static	Percent of stream lengths in the watershed which are third-order streams (Strahler order); from NHDPlus & percentage	percentage
	PCT_4TH_ORDER	static	Percent of stream lengths in the watershed which are fourth-order streams (Strahler order); from NHDPlus & percentage	percentage
	PCT_5TH_ORDER	static	Percent of stream lengths in the watershed which are fifth-order streams (Strahler order); from NHDPlus & percentage	percentage
	PCT_6TH_ORDER_OR_MORE	static	Percent of stream lengths in the watershed which are sixth or greater-order streams (Strahler order); from NHDPlus & percentage	percentage

Group	Name	Type	Description	Unit
Historical and current dams information	DDENS_2009	static	Dam density; number per 100 km sq	number of dams/100 km ²
	STOR_NOR_2009	static	Dam storage in watershed ("NORMAL_STORAGE"); megaliters total storage per sq km (1 megalitres = 1,000,000 liters = 1,000 cubic meters)	megaliters/km ²
NPDES	NPDES_MAJ_DENS	static	Density of NPDES (National Pollutant Discharge Elimination System) "major" point locations in the watershed; number per 100 km sq. Major locations are defined by an EPA-assigned major flag. From the download of NPDES national database summer 2006.	number of sites/100km ²
Percentages of land cover 2006 in the watershed and landscape	DEVNLCD06	static	Watershed percent "developed" (urban), 2006 era (2001 for AK-HI-PR). Sum of classes 21, 22, 23, and 24.	percentage
	FORESTNLCD06	static	Watershed percent "forest", 2006 era (2001 for AK-HI-PR). Sum of classes 41, 42, and 43.	percentage
	PLANTNLCD06	static	Watershed percent "planted/cultivated" (agriculture), 2006 era (2001 for AK-HI-PR). Sum of classes 81 and 82.	percentage
	WATERNLCD06	static	Watershed percent Open Water (class 11)	percentage
	WOODYWETNLCD06	static	Watershed percent Woody Wetlands (class 90)	percentage
	EMERGWETNLCD06	static	Watershed percent Emergent Herbaceous Wetlands (class 95)	percentage
Nitrogen and phosphorus application rate in the watershed	NITR_APP_KG_SQKM	static	Estimate of nitrogen from fertilizer and manure, from Census of Ag 1997, based on county-wide sales and percent agricultural land cover in the watershed.	kg/km ²
	PHOS_APP_KG_SQKM	static	Estimate of nitrogen from fertilizer and manure, from Census of Ag 1997, based on county-wide sales and percent agricultural land cover in the watershed.	kg/km ²
Pesticide	PESTAPP_KG_SQKM	static	Estimate of agricultural pesticide application (219 types), kg/sq km, from Census of Ag 1997, based on county-wide sales and percent agricultural land cover in the watershed	kg/km ²
Regions	ECO2_BAS_DOM	static	Dominant (highest % of the area) Level II ecoregion within the watershed. See X.Region_Names sheet for crosswalk to name.	unitless
	ECO3_BAS_DOM	static	Dominant (highest % of the area) Level III ecoregion within the watershed. See X.Region_Names sheet for crosswalk to name.	Level III ecoregion (1-84)
	NUTR_BAS_DOM	static	Dominant (highest % of the area) nutrient ecoregion within the watershed. See X.Region_Names sheet for crosswalk to name.	Nutrient ecoregion (1-14)
	HLR_BAS_DOM_100M	static	Dominant (highest % of the area) Hydrologic Landscape Region within the watershed. See X.Region_Names sheet for crosswalk to name.	HLR region (1-20)
	PNV_BAS_DOM	static	Dominant (highest % of the area) Potential Natural Vegetation (PNV) within the watershed. See X.Region_Names sheet for crosswalk to name.	PNV type (1-63)
Soil	AWCAVE	static	Average value for the range of available water capacity for the soil layer or horizon (inches of water per inch of soil depth)	unitless
	PERMAVE	static	Average permeability (inches/hour)	inches/hour
	BDAVE	static	Average value of bulk density (grams per cubic centimeter)	grams per cubic centimeter
	OMAVE	static	Average value of organic matter content (percent by weight)	percentage
	WTDEPAVE	static	Average value of depth to seasonally high water table (feet)	feet
	ROCKDEPAVE	static	Average value of total soil thickness examined (inches)	inches
	CLAYAVE	static	Average value of clay content (percentage)	percentage
	SILTAVE	static	Average value of silt content (percentage)	percentage
	KFACT_UP	static	Average K-factor value for the uppermost soil horizon in each soil component. K-factor is an erodibility factor which quantifies the susceptibility of soil particles to detachment and movement by water. The K-factor is used in the Universal Soil Loss Equation (USLE) to estimate soil loss by water. Higher values of the K-factor indicate greater potential for erosion	unitless
Topographic characteristics	RFACT	static	Rainfall and Runoff factor ("R factor" of Universal Soil Loss Equation); average annual value for the period 1971-2000.	100s ft-tonf in/h/ac/yr
	ELEV_MEAN_M.BASIN	static	Mean watershed elevation (meters) from 100m National Elevation Dataset	m
	SLOPE_PCT	static	Mean watershed slope, percent. Derived from 100m resolution National Elevation Dataset, so slope values may differ from those calculated from data of other resolutions.	percentage
Latitude and Longitude	ASPECT_DEGREES	static	Mean watershed aspect, degrees (degrees of the compass, 0-360). Derived from 100m resolution National Elevation Data. 0 and 360 point to north, because of the national Albers projection actual aspect may vary.	degrees (0-360)
	LAT.GAGE	static	Latitude at gage, decimal degrees	decimal degrees, datum NAD83
Snow	LNG.GAGE	static	Longitude at gage, decimal degrees	decimal degrees, datum NAD83
	SNOW_PCT_PRECIP	static	Snow percent of total precipitation estimate, mean for period 1901-2000. From McCabe and Wolock (submitted, 2008), 1km grid.	percentage